



Calibrating the temporal and spatial dynamics of the Ediacaran - Cambrian radiation of animals

Fred T. Bowyer^{a,b,*}, Andrey Yu Zhuravlev^c, Rachel Wood^b, Graham A. Shields^d, Ying Zhou^d, Andrew Curtis^b, Simon W. Poulton^a, Daniel J. Condon^e, Chuan Yang^e, Maoyan Zhu^{f,g}

^a School of Earth and Environment, University of Leeds, Leeds LS2 9JT, UK

^b School of GeoSciences, University of Edinburgh, James Hutton Road, Edinburgh EH9 3FE, UK

^c Department of Biological Evolution, Faculty of Biology, Lomonosov Moscow State University Leninskie Gory 1(12), Moscow 119234, Russia

^d Department of Earth Sciences, University College London, Gower Street, London WC1E 6BT, UK

^e British Geological Survey, Keyworth NG12 5GG, UK

^f State Key Laboratory of Palaeobiology and Stratigraphy, Nanjing Institute of Geology and Palaeontology and Center for Excellence in Life and Palaeoenvironment, Chinese Academy of Sciences, Nanjing 210008, China

^g College of Earth and Planetary Sciences, University of Chinese Academy of Sciences, Beijing 10049, China

ARTICLE INFO

Keywords:

Ediacaran
Cambrian
Evolution
Chronostratigraphy
Biostratigraphy
Chemostratigraphy
Carbon isotopes
Strontium isotopes
Temporal calibration
Geochronology

ABSTRACT

The Ediacaran-Cambrian transition, which incorporates the radiation of animals, lacks a robust global temporal and spatial framework, resulting in major uncertainty in the evolutionary dynamics of this critical radiation and its relationship to changes in palaeoenvironmental geochemistry. We first present a new $\delta^{13}\text{C}_{\text{carb}}$ composite reference curve for the Ediacaran Nama Group of southern Namibia, and we then outline four new possible global age models (A to D) for the interval 551–517 million years ago (Ma). These models comprise composite carbonate-carbon isotope ($\delta^{13}\text{C}_{\text{carb}}$) curves, which are anchored to radiometric ages and consistent with strontium isotope chemostratigraphy, and are used to calibrate metazoan distribution in space and time. These models differ most prominently in the temporal position of the basal Cambrian negative $\delta^{13}\text{C}_{\text{carb}}$ excursion (BACE). Regions that host the most complete records show that the BACE nadir always predates the Ediacaran-Cambrian boundary as defined by the first appearance datum (FAD) of the ichnospecies *Treptichnus pedum*. Whilst treptichnid traces are present in the late Ediacaran fossil record, the FAD of the ichnospecies *T. pedum* appears to post-date the last appearance datums (LADs) of in situ representatives of the skeletal organisms *Cloudina* and *Namacalathus* in all environments with high-resolution $\delta^{13}\text{C}_{\text{carb}}$ data. Two age models (A and B) place the BACE within the Ediacaran, and yield an age of ~ 538.8 Ma for the Ediacaran-Cambrian boundary; however models C and D appear to be the most parsimonious and may support a recalibration of the boundary age by up to 3 Myr younger. All age models reveal a previously underappreciated degree of variability in the terminal Ediacaran, incorporating notable positive and negative excursions that precede the BACE. Notwithstanding remaining uncertainties in chemostratigraphic correlation, all models support a pre-BACE first appearance of Cambrian-type shelly fossils in Siberia and possibly South China, and show that the Ediacaran-Cambrian transition was a protracted interval represented by a series of successive radiations.

1. Introduction

The late Ediacaran to early Cambrian interval encompasses the Gaskiers glaciation (~ 580 Ma), the first appearance of complex macroscopic life (~ 575 Ma), mobile biota (≤ 560 Ma), skeletal metazoans (~ 550 Ma), and the origin of modern metazoan phyla (Wood et al., 2019). Understanding the temporal and spatial context of these

events is currently limited due to the lack of high-resolution age models to allow correlation of key sections. The geological record throughout this interval also contains numerous unconformities and gaps of uncertain duration, a sparse global distribution of datable stratiform volcanic deposits, and diverse endemic biotas, resulting in loose chronostratigraphic and biostratigraphic control. As a result, no consistent global chronostratigraphic correlation exists, particularly for

* Corresponding author at: School of GeoSciences, University of Edinburgh, James Hutton Road, Edinburgh EH9 3FE, UK.

E-mail address: fred.bowyer@ed.ac.uk (F.T. Bowyer).

<https://doi.org/10.1016/j.earscirev.2021.103913>

Received 12 September 2021; Received in revised form 21 December 2021; Accepted 23 December 2021

Available online 30 December 2021

0012-8252/© 2021 The Author(s). Published by Elsevier B.V. This is an open access article under the CC BY license (<http://creativecommons.org/licenses/by/4.0/>).

the critical late Ediacaran to lower Cambrian (Fortunian Stage) interval. Early metazoans evolved in a highly dynamic Earth system, and so without a high-resolution temporal and spatial framework we are unable to address many profound uncertainties, including the evolutionary dynamics of the Cambrian Explosion, the response of metazoans to local and global changes in oceanic redox conditions and nutrient availability, and whether one or more contemporaneous mass extinctions occurred.

The formal placement of the Ediacaran-Cambrian boundary in the Fortune Head section, Newfoundland, Canada, which is based on the first appearance datum (FAD) of *Treptichnus pedum* ichnospecies (Brasier et al., 1994a), has been particularly problematic since it occurs in a section with few datable volcanics, sparse skeletal biota, and limited potential for chemostratigraphy (Babcock et al., 2014). Indeed, the choice of *T. pedum* as a marker fossil for the basal Cambrian has also been a source of contention given the strong environmental, lithological and facies dependency for preservation of this trace, resulting in its notable absence from carbonate-dominated successions (e.g. Babcock et al., 2014). A similar problem is encountered when attempting to define the basal Cambrian using the first appearance of ‘Cambrian-type’ small skeletal fossils, which are themselves absent or rare in siliciclastic-dominated successions, especially in environments that were not conducive to early phosphatization. To overcome this complication, a holistic integration of radiometric, chemostratigraphic and palaeontological data across this interval is crucial. At present, the age of the Ediacaran-Cambrian boundary is 541.0 ± 1.0 Ma (ICC 2021), however the radiometric age of a tuff deposit in the Nama Group, Namibia, on the Kalahari Craton, provides a current best estimate of 538.8 Ma for the maximum age of the first appearance of *T. pedum* (Linnemann et al., 2019; Xiao and Narbonne, 2020).

The carbon isotopic composition of marine carbonates ($\delta^{13}\text{C}_{\text{carb}}$) is most commonly considered to reflect secular changes in the ratio of ^{13}C to ^{12}C in seawater that are associated with changes in the relative export/burial rates of inorganic versus organic carbon (Kaufman et al., 1991; Keith and Weber, 1964; Veizer et al., 1980; Veizer and Hoefs, 1976). As a result, secular $\delta^{13}\text{C}_{\text{carb}}$ profiles have been used for regional and global correlation (Halverson et al., 2010; Macdonald et al., 2013; Maloof et al., 2010; Yang et al., 2021; Zhu et al., 2007). However, a number of local effects have also been proposed that may partially decouple the local record of primary $\delta^{13}\text{C}_{\text{carb}}$ from the composition of dissolved inorganic carbon (DIC) in the open ocean. These include diurnal coupling between photosynthesis and carbonate saturation in shallow carbonate settings (Geyman and Maloof, 2019), local DIC pools of distinct isotopic composition (Cui et al., 2020b; Melim et al., 2002), and the possibility for water-column methanogenesis and carbonate recycling under low-sulfate conditions associated with restriction (Cui et al., 2020b). Additionally, facies-specific diagenetic regimes can yield distinct $\delta^{13}\text{C}_{\text{carb}}$ for time-equivalent sections in modern marine basins (Melim et al., 2002), and this has also been established in the Cryogenian interglacial ocean (Hoffman and Lamothe, 2019), and the Paleoproterozoic Lomagundi-Jatuli event (Prave et al., 2021). As a result, changes in $\delta^{13}\text{C}_{\text{carb}}$ may in fact archive contemporaneous pools of DIC from adjacent depositional settings with variable carbon isotope composition. The potential for both local water column DIC and the effects of carbonate diagenesis to result in significant deviation of $\delta^{13}\text{C}_{\text{carb}}$ from global seawater $\delta^{13}\text{C}$ may therefore be problematic when building $\delta^{13}\text{C}_{\text{carb}}$ -based age frameworks.

Despite these potential complications, it is not clear why during certain intervals of geological history some depositional settings acquire $\delta^{13}\text{C}_{\text{carb}}$ values that deviate markedly from mean values (Hoffman and Lamothe, 2019). For example, integrated $\delta^{13}\text{C}_{\text{carb}}$, $\delta^{44}\text{Ca}$, $\delta^{26}\text{Mg}$ and sequence stratigraphic study of the Cryogenian interglacial Trezona $\delta^{13}\text{C}_{\text{carb}}$ excursion reveals that, whilst facies-specific trends in $\delta^{13}\text{C}_{\text{carb}}$ may correspond with fluid vs sediment buffered diagenesis, the excursion itself is of global significance and may correspond with global changes in siliciclastic vs carbonate sedimentation, nutrient delivery, and/or eustatic sea level (Ahm et al., 2021). Therefore, notwithstanding

uncertainties in the driving mechanisms for $\delta^{13}\text{C}_{\text{carb}}$ records and possible facies-related, diagenetic offsets, the secular trends represented by gradual unidirectional shifts in $\delta^{13}\text{C}_{\text{carb}}$ in multiple globally distributed and temporally equivalent open-marine sections may reflect changes to the carbon cycle that are of global significance, and hence are applicable for chemostratigraphic correlation.

To date, efforts to produce a global composite Ediacaran $\delta^{13}\text{C}_{\text{carb}}$ record (e.g. Macdonald et al., 2013; Yang et al., 2021) have revealed the middle Ediacaran Shuram negative anomaly at around $<579 - >564$ Ma (Rooney et al., 2020; Yang et al., 2021), followed by a positive shift from ca. 564–550 Ma. The sedimentary record from ca. 564–550 Ma is radiometrically well dated in Baltica (the East European Platform) (Yang et al., 2021) and Avalonia (Matthews et al., 2020; Noble et al., 2015); however, siliciclastic strata with poor $\delta^{13}\text{C}_{\text{carb}}$ resolution dominate these successions. A subsequent negative excursion with a recovery at ~550 Ma (Yang et al., 2021) is followed by a final late Ediacaran positive plateau (the EPIP, Zhu et al., 2017). This plateau appears to terminate with the onset of a globally widespread large magnitude (min $\delta^{13}\text{C}_{\text{carb}}$ of -10‰) negative excursion, termed ‘1n’ in strata of the Siberian Platform, and in previous global compilations (Kouchinsky et al., 2007; Maloof et al., 2010). This excursion is considered to be approximately coincident with the Ediacaran-Cambrian boundary and has also previously been termed the ‘Basal Cambrian negative $\delta^{13}\text{C}_{\text{carb}}$ excursion’ (BACE); an acronym that is adopted herein. The age of the BACE is currently correlated with a radiometrically dated negative excursion in the A4 Member of the Ara Group, Oman at ~541 Ma (Bowring et al., 2007; Hodgin et al., 2020; Maloof et al., 2010; Smith et al., 2015). Possible mass extinctions have been suggested between the Ediacaran White Sea and Nama biotic assemblages, and again at the Ediacaran-Cambrian boundary, coincident with the BACE (e.g. Amthor et al., 2003; Darroch et al., 2018).

Determining the global nature and age of the BACE has been particularly problematic, but is critical for developing a robust biostratigraphic and chronostratigraphic framework across this interval. The BACE reaches a $\delta^{13}\text{C}_{\text{carb}}$ nadir of -10‰ and has been recorded in all fossiliferous successions with high-resolution $\delta^{13}\text{C}_{\text{carb}}$ data, except the Nama Group. The FAD of *T. pedum* occurs above the BACE in all regions that host both features (e.g. Smith et al., 2015, 2016; Hodgin et al., 2020). As a radiometric basis for the age of the Ediacaran-Cambrian boundary derives from the Nama Group (Linnemann et al., 2019; Xiao and Narbonne, 2020), the position of the BACE (if present) in the Nama succession must be determined. Recent high precision radiometric and $\delta^{13}\text{C}_{\text{carb}}$ data from Laurentia appear to constrain the age of the BACE nadir to ≤ 539.4 Ma, coincident with stable positive $\delta^{13}\text{C}_{\text{carb}}$ data on the Kalahari craton (Hodgin et al., 2020). It has therefore been suggested that the conflicting $\delta^{13}\text{C}_{\text{carb}}$ trends between the Laurentian and Kalahari datasets may result from local pools of dissolved inorganic carbon (DIC) with distinct isotopic compositions (Hodgin et al., 2020). In order to test whether data are unrepresentative of global $\delta^{13}\text{C}_{\text{carb}}$, it is first necessary to discount all alternative possibilities associated with uncertainties in the $\delta^{13}\text{C}_{\text{carb}}$ age model framework.

Here, we present an updated $\delta^{13}\text{C}_{\text{carb}}$ framework for the Ediacaran Nama Group of southern Namibia. These data are first correlated regionally by combined litho-, chemo-, and sequence stratigraphy, then constrained in time using published high precision U-Pb ages determined via zircon chemical abrasion isotope dilution thermal ionization mass spectrometry (CA-ID-TIMS). We correlate trends in the resulting Nama reference curve with $\delta^{13}\text{C}_{\text{carb}}$ data from globally distributed sections that are well constrained by interbedded zircon U-Pb CA-ID-TIMS ages, and robust high-resolution regional section correlation, for the interval ~ 551–538.5 Ma. The $\delta^{13}\text{C}_{\text{carb}}$ record is then extended to 517 Ma in multiple regions with high resolution litho-, chemo-, and sequence stratigraphic records. Compiled data from sections that host the most robust radiometric constraints throughout this interval act as framework curves to reveal trends in the global data that can be confidently constrained in age. These curves are used to anchor a wider correlation in

order to best fit high-resolution $\delta^{13}\text{C}_{\text{carb}}$ data from key sections that lack robust radiometric constraints.

This allows construction of four possible composite carbon isotope curves and age models, comprising 130 globally distributed sections (Australia, Brazil, Kazakhstan, Mongolia, Morocco, Namibia, Mexico, USA, Canada, Oman, Siberia and South China). These curves are consistent with all reliable radiometric age data and strontium isotope ($^{87}\text{Sr}/^{86}\text{Sr}$) records between ~551–517 Ma (Tables S1 and S2). All models reveal a previously underappreciated degree of variability in the EPIP, incorporating multiple positive and negative excursions preceding the BACE that are globally widespread. Differences between the four age models result from ongoing uncertainties which we review in detail. All FADs and, for Ediacaran taxa, Last Appearance Datums (LADs) of key fossil occurrences are calibrated within this framework (Tables S2 and S3). This provides the basis for biotic temporal and spatial distributions to be accurately constrained and visualized.

2. Constructing a $\delta^{13}\text{C}_{\text{carb}}$ reference curve for the Nama Group, Kalahari Craton

The Nama Group in Namibia and South Africa, comprises a richly-fossiliferous mixed carbonate-siliciclastic succession deposited in a foreland basin on the Kalahari Craton. The succession developed during flexural subsidence associated with two major orogenies; the Damara to the north, and the Gariep to the southwest (Germis, 1983; Germis and Gresse, 1991; Gresse and Germis, 1993) (Fig. 1). Near-complete exposure and minimal structural deformation across hundreds of square kilometers have inspired half a century of detailed sedimentological and palaeontological research, incorporating high resolution litho-, chemo- and sequence stratigraphy (Darroch et al., 2015; Darroch et al., 2021; Jensen et al., 2000; Saylor, 2003; Saylor et al., 1998; Smith, 1998; Wood et al., 2015). These aspects, in combination with high-precision radiometric age calibration (Bowring et al., 2007; Grotzinger et al., 1995; Linnemann et al., 2019), make the Nama Group the best candidate succession globally for construction of a terminal Ediacaran $\delta^{13}\text{C}_{\text{carb}}$ reference curve. This is especially the case for the lower Nama Group (Kuibis Subgroup), where carbonate ramp deposits are ubiquitous throughout the northern (Zaris) sub-basin.

$\delta^{13}\text{C}_{\text{carb}}$ data from fourteen sections of the Nama Group, Namibia (Saylor et al., 1995; Smith, 1998; Wood et al., 2015), compiled within a sequence stratigraphic framework and calibrated to dated volcanic tuff interbeds, result in a composite Ediacaran Nama $\delta^{13}\text{C}_{\text{carb}}$ reference curve (Fig. 1). Gaps in the $\delta^{13}\text{C}_{\text{carb}}$ record of individual sections are permitted at exposure or erosion surfaces, or during significant intervals of siliciclastic deposition. Below, we explore implications for global correlation of the $\delta^{13}\text{C}_{\text{carb}}$ reference curve derived for the Kuibis (ca. 551–546 Ma) and Schwarzrand (<546–538 Ma) subgroups.

2.1. The Kuibis Subgroup

In the Kuibis Subgroup succession, positive, laterally consistent $\delta^{13}\text{C}_{\text{carb}}$ values in the lower Hoogland Member (Zaris Formation) of the Zaris sub-basin are constrained by a zircon U-Pb CA-ID-TIMS age of 547.36 ± 0.23 Ma (Bowring et al., 2007) (Fig. 1). Carbonate strata in multiple sections below this ash bed record a gradual recovery from a negative $\delta^{13}\text{C}_{\text{carb}}$ excursion. This can be readily correlated with the $\delta^{13}\text{C}_{\text{carb}}$ trend expressed in strata of the lower Dengying Formation, South China (see section 5.2). Recovery from this negative $\delta^{13}\text{C}_{\text{carb}}$ excursion in the lower Dengying Formation is constrained by a zircon U-Pb CA-ID-TIMS age of 550.1 ± 0.6 Ma (Yang et al., 2021, updated from 551.09 ± 1.02 Ma, Condon et al., 2005) from an ash bed in the underlying Miaohe Member at Jijiawan (/Jiuqunao) section (Table S1). The age of the 0‰ crossing point in the lower Kuibis Subgroup can therefore be anchored to ~550 Ma. The preceding negative excursion (≥ 550 Ma), whilst present and radiometrically calibrated in South China, is expressed most completely and with highest resolution in multiple

sections by carbonates of the Dabis Formation in both the Zaris and Witputs sub-basins of the Nama Group. This is a recently recognized distinct negative $\delta^{13}\text{C}_{\text{carb}}$ excursion (Yang et al., 2021), herein termed the basal Nama excursion (BANE, Fig. 1b).

Subsequent to the BANE, peak $\delta^{13}\text{C}_{\text{carb}}$ values are reached within the upper Omkyk Member of the Zaris Formation, and lower members of the Dengying Formation. This $\delta^{13}\text{C}_{\text{carb}}$ peak is herein termed the Omkyk excursion (OME, Fig. 1b).

The onset of a gradual decline prior to 547.32 ± 0.31 Ma (Bowring et al., 2007) is constrained by a tuff bed within the lower Hoogland Member of the upper Zaris Formation and correlative intervals of the lower Dengying Formation (Table S2). Declining $\delta^{13}\text{C}_{\text{carb}}$ values culminate in a short-lived (<0.5 Ma) negative excursion, with a recovery to ~0‰ recorded at 546.72 ± 0.21 Ma by a tuff bed in the middle A0 Member of the Ara Group, Oman (see section 5.5, Bowring et al., 2007; Schmitz, 2012). This minor negative excursion is expressed in carbonate interbeds of the Urikos Member of the Zaris Formation, Namibia, and the A0 Member of the Ara Group, Oman (Bowring et al., 2007; Saylor et al., 1998). It may also correspond with a minor negative excursion recorded in the lower Khatyspyt Fm of the northern Siberian Platform (Cui et al., 2016a; Knoll et al., 1995), although this remains uncertain (see section 5.3).

Based on the interbasinal $\delta^{13}\text{C}_{\text{carb}}$ correlation herein (Fig. 1) and published palaeontological information, carbonates in the lower Kuibis Subgroup (Mara Member of the Dabis Fm) of the Witputs sub-basin host the earliest FAD of *Cloudina* (Germis, 1983). This FAD may predate the 0‰ recovery from the BANE, however the precise location of the section that hosts the Mara Member cloudinids and associated $\delta^{13}\text{C}_{\text{carb}}$ data is undocumented. In the Zaris sub-basin, the earliest recorded appearance of cloudinids occurs immediately above the 0‰ recovery from the BANE (~550 Ma) within the lowermost upper Omkyk Member (Fig. 1). Siliciclastics in the lower Kuibis Subgroup (Kliphoek Member of the Dabis Formation) of the Witputs sub-basin, deposited immediately below the 0‰ recovery from the BANE, contain a rich fossil archive of soft-bodied biota (Maloney et al., 2020). The majority of the soft-bodied fossils in this interval correspond to the Nama assemblage, however this level may also host the regional last appearance of elements of the White Sea assemblage, including *Ausia fenestrata* (Hahn and Pflug, 1985; Pickford, 1995). Fossil impressions interpreted as *Ausia* have previously been noted from the middle Verkhovka Formation of the White Sea area (Grazhdankin, 2004), below a volcanic tuff in the overlying lower Zimmie Gory Formation recently redated to 552.96 ± 0.19 (Yang et al., 2021) (Table S1).

2.2. The Schwarzrand Subgroup

During deposition of the Schwarzrand Subgroup the locus of carbonate sedimentation shifted to the Witputs sub-basin, and siliciclastic deposits of the Zaris sub-basin record gradual basin infill (Germis, 1983; Gresse and Germis, 1993). The existing $\delta^{13}\text{C}_{\text{carb}}$ record of the Schwarzrand Subgroup consists of a low resolution $\delta^{13}\text{C}_{\text{carb}}$ dataset from the Huns and lower Spitskop members of the Urusis Formation, and multiple datasets of varying resolution from the upper Spitskop Member at Farm Swartpunt (Linnemann et al., 2019; Saylor et al., 1998; Wood et al., 2015). We present new $\delta^{13}\text{C}_{\text{carb}}$ data for two sections from the Urusis Fm (Nord Witputz and Swartpunt), and construct a composite lithostratigraphic and chemostratigraphic column incorporating available data from the lower Spitskop Member (Saylor et al., 1998) (Fig. 2).

Shallow marine facies of the lower Huns Member at Nord Witputz show initially high $\delta^{13}\text{C}_{\text{carb}}$ values (max = 4.24‰) that gradually decrease to reach 0.08‰ near the top of the section (Fig. 2). Higher order variability in the $\delta^{13}\text{C}_{\text{carb}}$ data of the lower Huns Member may be associated with a series of parasequences, where lower $\delta^{13}\text{C}_{\text{carb}}$ reflects deepening of the depositional environment. Samples of both shallow and marginally deeper facies show pronounced and simultaneous decreases in their mean $\delta^{13}\text{C}_{\text{carb}}$ composition up-section, which may reflect

Fig. 1. Sequence stratigraphic and carbon isotope chemostratigraphic correlation of the Nama Group, Namibia with resulting reference curve for the Kalahari craton for the interval ~ 550–538.5 Ma (Saylor et al., 1998; Smith, 1998; Wood et al., 2015). (a) Litho-, chemo- and sequence stratigraphic correlation for sections of the Zaris sub-basin after Smith (1998) and Wood et al. (2015). New data for sections 12 and 14. (b) Resulting Nama $\delta^{13}\text{C}_{\text{carb}}$ reference curve showing position of tuff bed age constraints and sequence boundaries. Note that age model between ca. 547 Ma and 540 Ma remains poorly constrained. BANE: Basal Nama Excursion, OME: Omkyk Excursion, A0, A3 and A4 named after tentative correlation with radiometrically dated excursions in the A0, A3 and A4 members of the Ara Group, Oman (see text for details). BACE-A, B and C correlate to the positions of the 1n/BACE in models A, B and C, respectively (Table S2). See Fig. 2 for key to lithology and sequence stratigraphy. Radiometric data ($^{238}\text{U}/^{206}\text{Pb}$ CA-ID-TIMS) are from (Bowring et al., 2007; Linnemann et al., 2019) and italicized data (air abrasion ID-TIMS $^{207}\text{Pb}/^{206}\text{Pb}$) are from Grotzinger et al. (1995) recalculated in Schmitz (2012) (the age of tuff bed 5 is discounted; details in Table S1). See Fig. S1 for a high-resolution version of this figure.

a gradual trend in seawater $\delta^{13}\text{C}_{\text{carb}}$ overprinted by minor perturbations associated with regional facies. Based on regional stratigraphic correlation, the Urusis Fm of the Witputs sub-basin was deposited equivalent to siliciclastic deposits of the Schwarzrand Subgroup in the Zaris sub-basin (Germs, 1983), and is therefore likely to be younger than ~546 Ma (Fig. 1).

The lower Spitskop Member contains a volcanic tuff deposit with a $^{207}\text{Pb}/^{206}\text{Pb}$ age of 542.68 ± 1.25 Ma (Grotzinger et al., 1995, recalculated in Schmitz, 2012) (Table S1). Carbon isotope data of relatively low resolution have previously been presented for the lower Spitskop Member from the lower part of a composite section described as ‘near Swartkloofberg’ (Saylor et al., 1998) (Fig. 2). The lower part of this section (corresponding to medium scale sequences D11 – E16 of Saylor, 2003) lies to the north of our Huns Member section, and the upper part (medium scale sequences E17 and E18 of Saylor, 2003) corresponds to the Swartpunt section (Fig. 2, and see Fig. 1 of Saylor and Grotzinger, 1996). According to Saylor (2003), a total thickness of ~370 m of interbedded shale and carbonate, for which only 18 data points are currently published, separates the Huns Member at Nord Witputz from the upper Spitskop Member at Swartpunt (Fig. 2) (Saylor et al., 1998). However, an alternative correlation for the relative position of the lower Spitskop Member data is discussed in the Supplementary Information. Future high resolution resampling for $\delta^{13}\text{C}_{\text{carb}}$, in addition to re-dating of ash beds throughout the lower Spitskop Member southeast of Swartpunt using the updated CA-ID-TIMS methodology, should yield valuable information to better constrain this interval in the global age model.

3. Developing age models and the stratigraphic position of the BACE in Namibia

3.1. The terminal Ediacaran (546–541 Ma)

The $\delta^{13}\text{C}_{\text{carb}}$ record between 546 Ma and 543 Ma remains poorly constrained globally due to a dearth of $\delta^{13}\text{C}_{\text{carb}}$ data interbedded with tuff beds dated by reliable radiometric methods (Fig. 3a). However, when the new $\delta^{13}\text{C}_{\text{carb}}$ data of the Huns Member are compared to other $\delta^{13}\text{C}_{\text{carb}}$ profiles from ca. 546–543 Ma from other cratons (e.g. Yangtze Block, Laurentia, Amazonia and Siberia, Fig. 3), the magnitude and overall trend in the data are consistent with a temporal position coincident with the initial downturn from positive values of up to 5‰ recorded in the middle Member of the Dengying Formation (Gaojiashan Member and equivalent units). We stress that this is a maximum age estimate based on the assumption that the age constraint from the overlying lower Spitskop Member (542.68 ± 1.25 Ma, Grotzinger et al., 1995, updated in Schmitz, 2012) approximates the true age of the lower Spitskop Member (see Supplementary Text for further discussion). A subsequent recovery to a positive $\delta^{13}\text{C}_{\text{carb}}$ peak is well constrained by 5 radiometric ages; 543.40 ± 3.5 Ma from the Baimatuo Member of the Yangtze Platform (Huang et al., 2020), 542.90 ± 0.12 Ma and 542.33 ± 0.11 Ma from the lower and upper A3 Member of the Ara Group (Bowring et al., 2007), and 542.37 ± 0.28 Ma and 541.85 ± 0.75 Ma from the upper Tamengo Formation, Brazil (Parry et al., 2017). Here, $\delta^{13}\text{C}_{\text{carb}}$ values increase once more to 3–5.6‰ (herein termed the ‘A3’ anomaly, Fig. 3) and then decline to a plateau of 0–2‰ prior to 541 Ma (Tables S1 and S2). The available data from the lower Spitskop Member, though sparse, correlate with predominantly positive $\delta^{13}\text{C}_{\text{carb}}$ values

that precede the negative excursion recorded in the A4 Member of the Ara Group (Fig. 3).

There are three possible positions for the BACE in the Nama Group, all of which are consistent with available radiometrically-dated tuff deposits and occur in siliciclastic units without $\delta^{13}\text{C}_{\text{carb}}$ data (Fig. 2). These give rise to three alternative age models A, B and C (Fig. 3). In each, we assume that the age of the A4 Member accurately constrains the $\delta^{13}\text{C}_{\text{carb}}$ excursion recorded in the A4 Member, as shown by Bowring et al. (2007) (see section 5.5 for further discussion of the Ara Group age model). For ease of distinction, the excursion in the A4 Member is herein termed the ‘A4 anomaly’. The position of the BACE in relation to the Spitskop Member is inferred either within the shale interval of medium scale sequence E17, stratigraphically beneath the ca. 540 Ma tuff bed at the base of the Swartpunt section (Model A), within the shale interval of medium scale sequence E18 above the well dated horizon constrained by multiple tuff deposits at ca. 539.6 Ma (Linnemann et al., 2019) (Model B), or in strata younger than the Swartpunt section (<538 Ma, Model C) (Figs. 2, 3).

Models A and B are consistent with a recent radiometric constraint from the La Ciénega Formation, Mexico (Hodgin et al., 2020). However, models B and C imply that the A4 anomaly does not correspond to the BACE, but rather to an earlier negative excursion with a recovery at or before ca. 540 Ma (Fig. 3c and d). In models A and B, the apparent absence of the BACE nadir in the Nama Group is interpreted simply as a function of coincident deposition of outer shelf shale for which $\delta^{13}\text{C}_{\text{carb}}$ data are lacking (Fig. 2). Indeed, if the A4 anomaly is of global significance and correctly constrained in time (see section 5.5), it is sequestered within a shale interval stratigraphically beneath the Swartpunt section in all models.

3.2. $^{87}\text{Sr}/^{86}\text{Sr}$ chemostratigraphy of the Ediacaran-Cambrian transition

Matching $\delta^{13}\text{C}_{\text{carb}}$ excursions in fossiliferous Ediacaran sections that display one or more $\delta^{13}\text{C}_{\text{carb}}$ excursions but lack radiometric ages is complicated by the finding here of multiple global late Ediacaran $\delta^{13}\text{C}_{\text{carb}}$ excursions. This is equally problematic for the multiple excursions present in the Fortunian Stage of the lower Cambrian. In an attempt to address this issue, we compile a further database of published $^{87}\text{Sr}/^{86}\text{Sr}$ data as an independent chronostratigraphic test (Table S2, Fig. 4). These $^{87}\text{Sr}/^{86}\text{Sr}$ data have been screened on a case-by-case basis using available geochemical data to account for modification of the Sr isotope composition associated with diagenetic alteration or common Rb (see Supplementary Text, Table S2). Reliable $^{87}\text{Sr}/^{86}\text{Sr}$ data are anchored directly to the prescribed age of the corresponding $\delta^{13}\text{C}_{\text{carb}}$ value in the same sample. In this way, we are able to constrain trends that we consider the most robust estimate of seawater $^{87}\text{Sr}/^{86}\text{Sr}$ composition, and use $^{87}\text{Sr}/^{86}\text{Sr}$ as an independent chronostratigraphic indicator for age models A, B and C for sections that lack radiometric ages (Fig. 4).

Revision of the age of the Shuram excursion after Rooney et al. (2020) and Yang et al. (2021) results in a highly uncertain interval (‘WSI’ in Figs. 3, 4) where $^{87}\text{Sr}/^{86}\text{Sr}$ data are largely unconstrained with the possible exception of values corresponding to the Blueflower Formation of NW Canada (Narbonne et al., 1994). The resulting late Ediacaran $^{87}\text{Sr}/^{86}\text{Sr}$ record (~551–538 Ma) is characterised by values that are relatively invariant about 0.70842–0.70846, and these values are

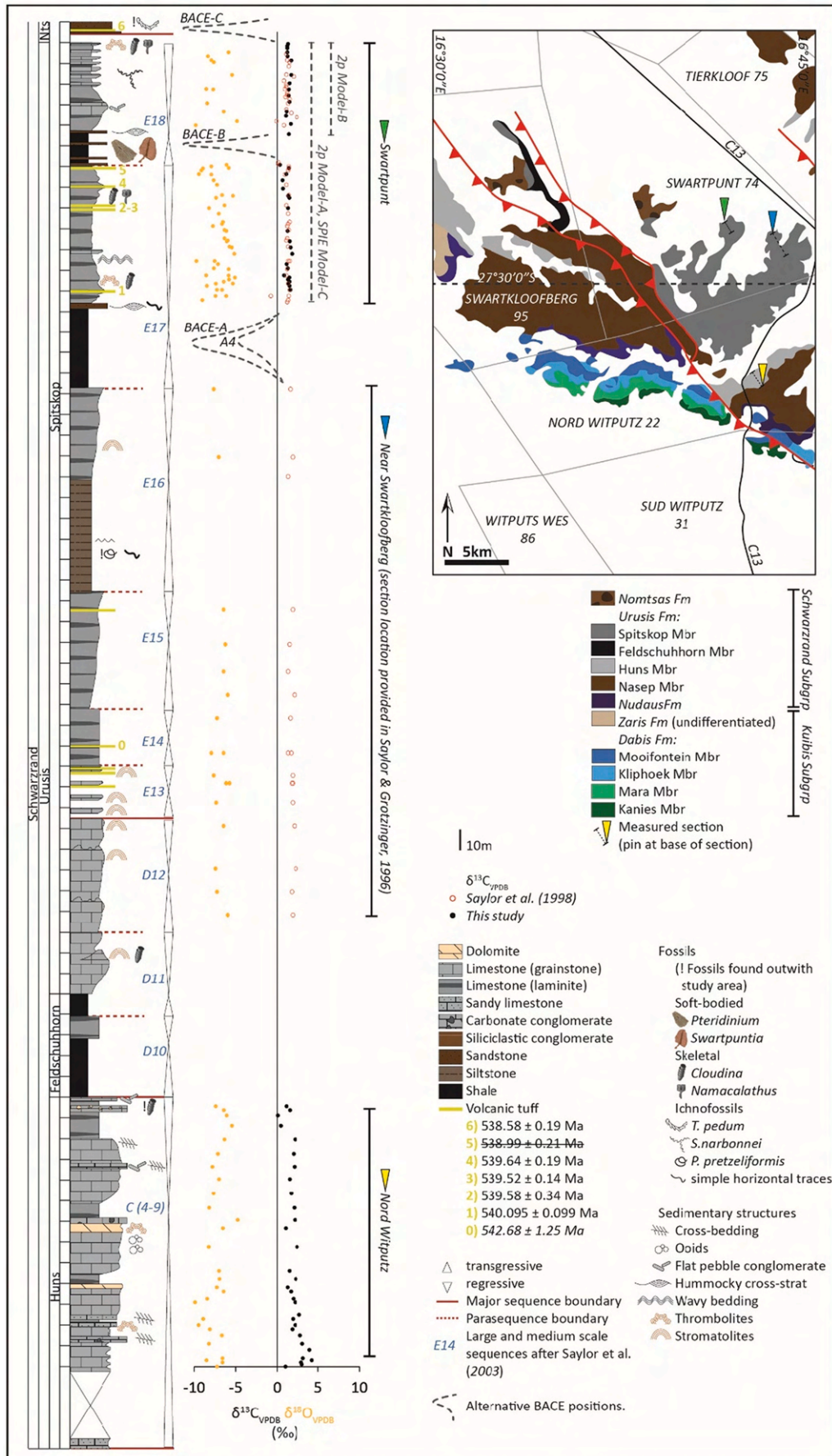


Fig. 2. Geological map and sampled sections of the Urusis Formation, Nama Group, southern Namibia. Composite section after Saylor (2003). Geological map shows relative positions of measured sections. Map redrawn from Saylor and Grotzinger (1996) using the 1:250000 map of Ai-Ais (2716), Geological Survey of Namibia, Ministry of Mines and Energy. Radiometric data ($^{238}U/^{206}Pb$ CA-ID-TIMS) are from Linemann et al. (2019) and italicized data (air abrasion ID-TIMS $^{207}Pb/^{206}Pb$) are from Grotzinger et al. (1995) recalculated in Schmitz (2012) (the age of tuff bed 5 is discounted; details in Table S1). BACE-A, B and C correlate to the positions of the 1n/BACE in models A, B and C, respectively (Table S2).

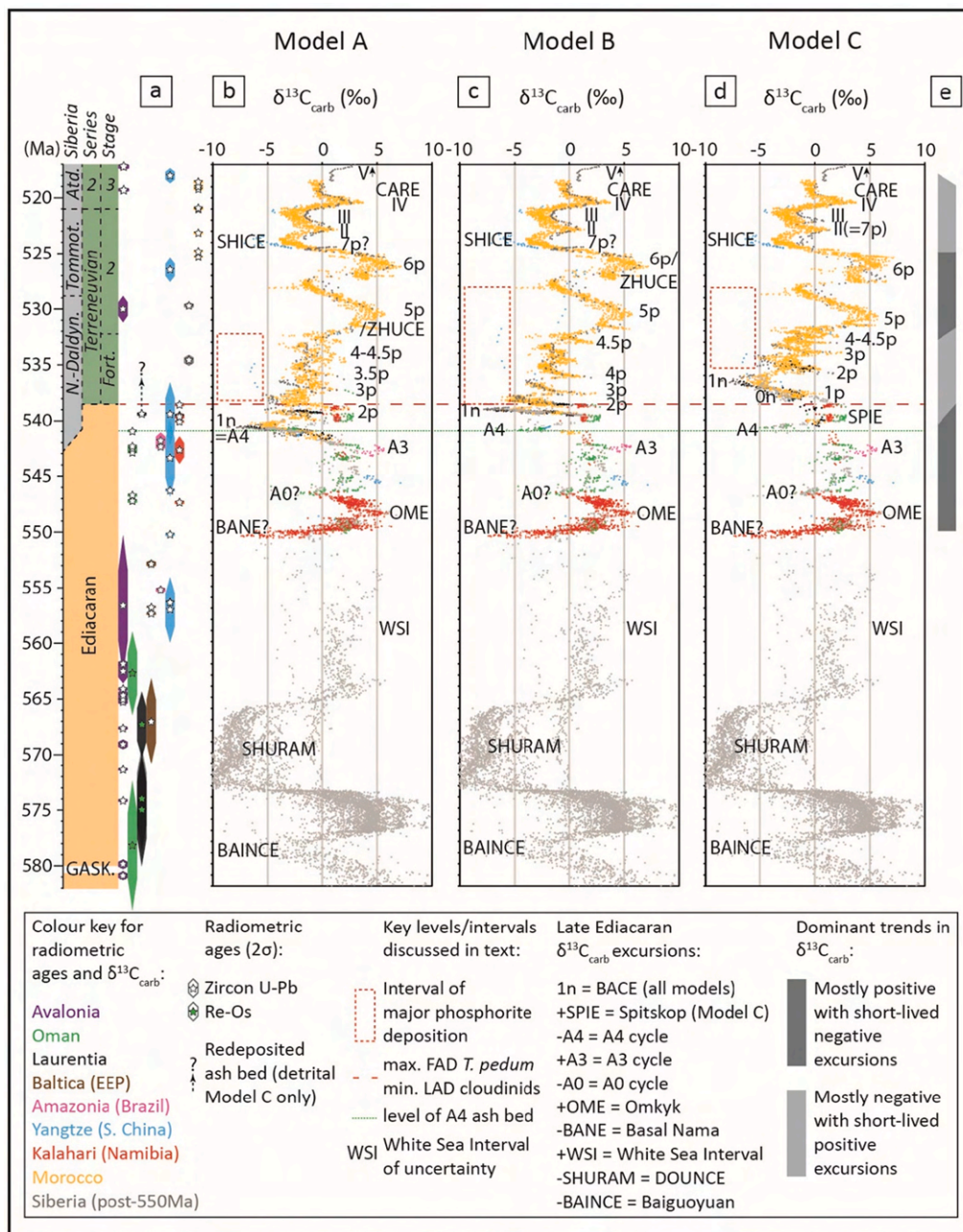


Fig. 3. Carbon isotope chemostratigraphic correlation models A–C. Ediacaran $\delta^{13}\text{C}_{\text{carb}}$ data are only presented for sections that are anchored by associated radiometric ages (e.g. Swartpunt), or where high resolution $\delta^{13}\text{C}_{\text{carb}}$ data are confidently correlated regionally to sections that contain radiometrically dated beds (e.g. La Ciénege Fm and Kuibis Subgroup sections). All data are coloured by craton (or region). Age model for 582–550 Ma interval in grey after Yang et al. (2021). (a) Available radiometric ages with associated internal/analytical uncertainty. See Supplementary Materials (Tables S1 and S2) for references to radiometric and $\delta^{13}\text{C}_{\text{carb}}$ data, in addition to biostratigraphic and section information. BANE marks the basal Nama negative $\delta^{13}\text{C}_{\text{carb}}$ excursion, OME marks the positive $\delta^{13}\text{C}_{\text{carb}}$ peak recorded in the Omkyk Member of the Zaris Formation of the Nama Group, Namibia. A0, A3 and A4 mark the relative positions of $\delta^{13}\text{C}_{\text{carb}}$ excursions with radiometric ages in the Ara Group, Oman. $\delta^{13}\text{C}_{\text{carb}}$ peaks 1p–6p, and I–V are labelled after direct correlation with the Sukharikha River section and Lena River sections of Siberia (e.g. Kouchinsky et al., 2007). 1n is equivalent to the BACE in all models.

consistent between Namibia, South China, Mongolia and southeastern Siberia (Table S2). The Khatyspyt Formation yields inconsistent outlier values down to 0.70784 (boxed data in Fig. 4b-d), accompanied by a high degree of scatter in $\delta^{13}\text{C}_{\text{carb}}$. The position of the Khatyspyt Formation remains problematic due to uncertainties in the nature of the boundary with the overlying Turkut Formation (see section 5.3). However, we consider the correlation proposed herein to be a reasonable estimate based on consistent $\delta^{13}\text{C}_{\text{carb}}$ trends between the Khatyspyt Formation and globally distributed sections throughout this interval. $^{87}\text{Sr}/^{86}\text{Sr}$ values remain constant throughout much of the Fortunian, but begin to decline approximately coincident with rising $\delta^{13}\text{C}_{\text{carb}}$ values in Cambrian Stage 2, reaching a nadir of ~ 0.70805 near the boundary between stages 2 and 3, prior to gradual recovery during upper Stage 3.

3.3. Incorporating additional section data

In order to test the validity of our Nama reference curve for global

$\delta^{13}\text{C}_{\text{carb}}$ correlation, and to explore the three alternative age models, we expand our dataset to incorporate published data from correlative strata into the early Cambrian from other cratons and regions (e.g. Yangtze Block, Oman, Laurentia, Amazonia, Morocco, Siberia, Mongolia, Fig. 3). We first prioritise sections with $\delta^{13}\text{C}_{\text{carb}}$ data and interbedded volcanic deposits dated via zircon U-Pb CA-ID-TIMS. Values of $\delta^{13}\text{C}_{\text{carb}}$, anchored by the age of interbedded tuff deposits (within internal/analytical uncertainty) provide the scaffold for wider correlation, and intervals that lack constraint from radiometric ages are considered to be the most uncertain (Tables S1 and S2). Within this framework, we utilize regional sequence stratigraphic models that incorporate gaps in the carbon isotope record of individual sections, due to unconformities or intervals of siliciclastic deposition, while excluding unreasonable sedimentation rates for given tectonic settings (Table S2). Individual sections are subdivided into units of consistent lithofacies, and relative sedimentation rates are permitted to vary accordingly (Table S2). Deeper marine carbonate facies (e.g. organic-rich thinly bedded limestone laminae) and

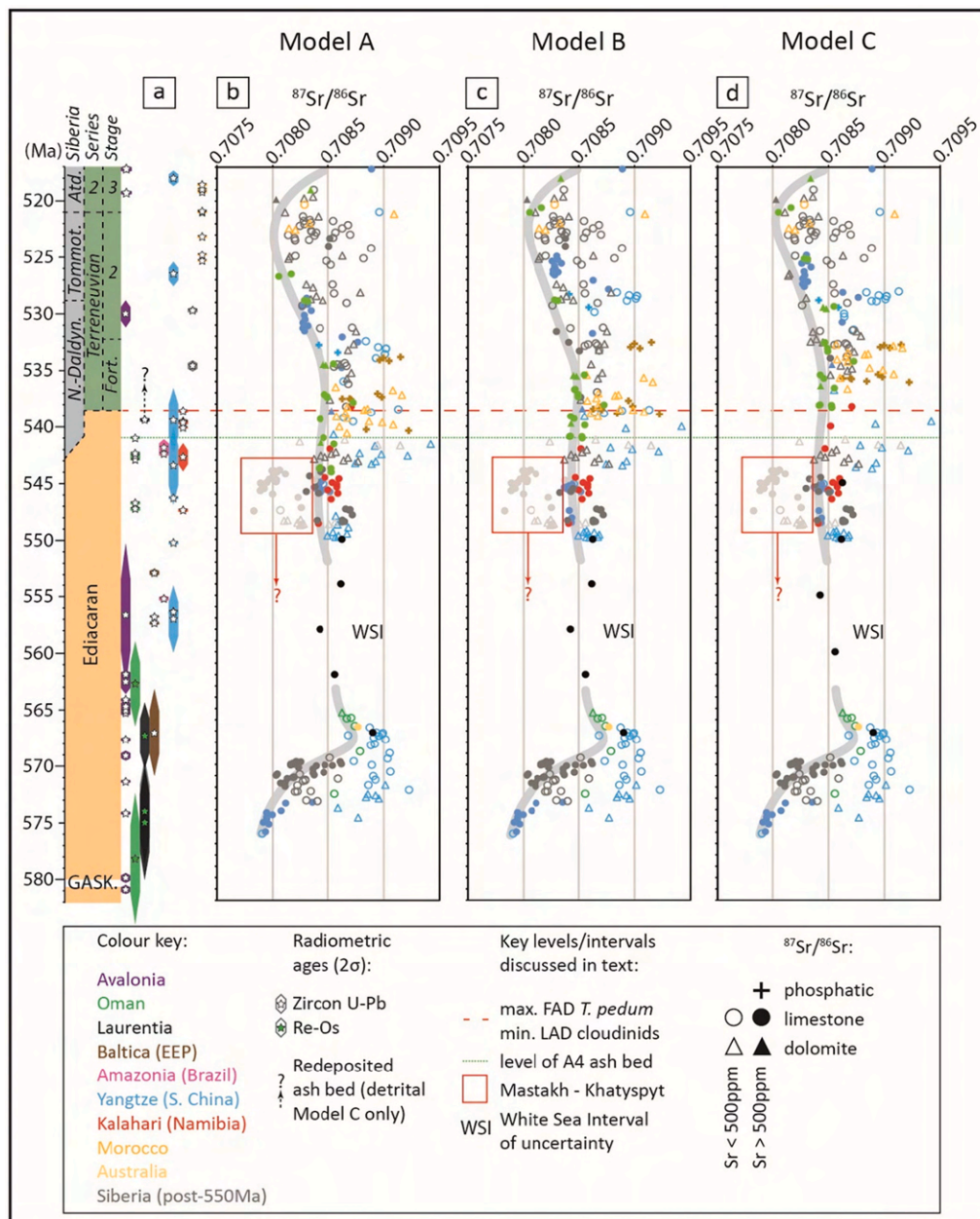


Fig. 4. Sr isotope chemostratigraphy with associated radiometric ages (a) resulting from carbon isotope chemostratigraphy after Model A (b), Model B (c) and Model C (d) for the interval ~576–517 Ma. Red boxes highlight unusually depleted values of the Mastakh and Khatyspyt formations. Data coloured according to craton (or region). (For interpretation of the references to colour in this figure legend, the reader is referred to the web version of this article.)

intervals of phosphorite deposition typically exhibit lower rates of deposition than shallow marine carbonate facies (e.g. dolostone and oolitic limestone deposited above fair weather wave base) within each region (Table S2).

Several high resolution $\delta^{13}\text{C}_{\text{carb}}$ correlation frameworks have been assembled for the lower Cambrian (e.g. Brasier et al., 1994b; Knoll et al., 1995; Kouchinsky et al., 2017, Kouchinsky et al., 2007, Kouchinsky et al., 2005; Maloof et al., 2010; Smith et al., 2015, Table S2). Our new framework is consistent with that derived by Maloof et al. (2010), but updates their model through incorporation of more recent high resolution $\delta^{13}\text{C}_{\text{carb}}$ datasets (e.g. Kouchinsky et al., 2017; Smith et al., 2015) and radiometric constraints (e.g. Hodgkin et al., 2020; Landing et al., 2020; Linnemann et al., 2019). We also consider updated biostratigraphic information integrated with $\delta^{13}\text{C}_{\text{carb}}$ from sections in South China (Steiner et al., 2020), Australia (Betts et al., 2018) and Laurentia

(Dilliard et al., 2007).

All global $\delta^{13}\text{C}_{\text{carb}}$ correlation models reveal widespread, but short-lived, negative excursions in an interval dominated by positive $\delta^{13}\text{C}_{\text{carb}}$ values in the terminal Ediacaran ~551–538 Ma (Fig. 3e). These models differ most prominently in their correlation of the BACE nadir, either within the latest Ediacaran (models A and B) or within the lowermost Cambrian (Model C), as defined by its position relative to the radiometric age that currently constrains the FAD of *T. pedum* in Namibia (Fig. 3). However, *T. pedum* has not been reported in strata older than the BACE nadir in any region that hosts the BACE, and so the BACE nadir may in fact be older than the Ediacaran-Cambrian boundary in all models (discussed further below). Models B and C offer valid alternatives to the generally accepted Model A that are consistent with radiometric (models B and C) and stratigraphic (Model C) information in all regions. The relative likelihood of each of these three models, and

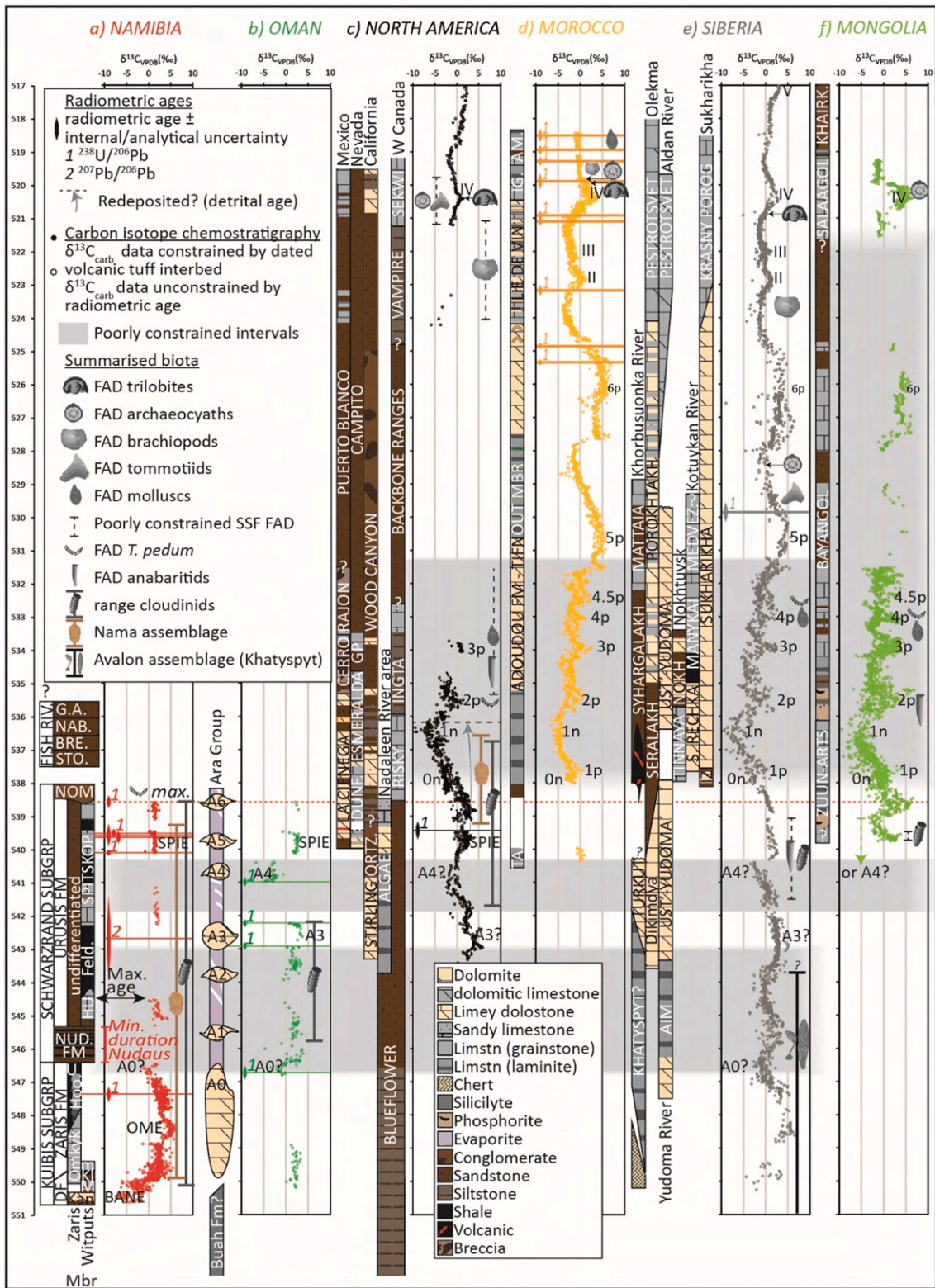


Fig. 5. High-resolution age model correlation by region for Model C only. Grey shading represents intervals of greatest uncertainty (see text for details). As in Fig. 3, the excursion marked as 1n represents the BACE. See Fig. S2 for a high resolution version of this figure.

their biostratigraphic implications, are further discussed below.

4. Implications for the age of the BACE and the Ediacaran-Cambrian boundary

The A4 anomaly records minimum $\delta^{13}C_{carb}$ values of -5% and one

outlier value of -6.7% (Amthor et al., 2003; Bowring et al., 2007) (Figs. 3 and 5). The onset of this negative excursion is anchored by an age of 541.00 ± 0.13 Ma (Bowring et al., 2007). The overlying A5 Member of the Ara Group records stable positive values of $2-3\%$, prior to the onset of another negative excursion (Amthor et al., 2003). The radiometric age of the A4 Member has been used to constrain an onset

age for the BACE of ~ 541 Ma (Model A, e.g. Bowring et al., 2007; Hodgin et al., 2020; Linnemann et al., 2019; Maloof et al., 2010). As previously noted, the BACE reaches a nadir of -10‰ and is recorded in all fossiliferous successions with high-resolution $\delta^{13}\text{C}_{\text{carb}}$ data, except the Nama Group, Namibia (Figs. 3 and 5, Table S2). A maximum age of 539.40 ± 0.23 Ma derives from a sandy dolostone bed in the La Ciénega Formation, Mexico, which lies within negative $\delta^{13}\text{C}_{\text{carb}}$ values inferred to correspond to the BACE interval (Tables S1 and S2, Hodgin et al., 2020). However, strata of the upper Spitskop Member of the Urusis Formation (Nama Group, southern Namibia) at the Swartpunt section record relatively stable positive $\delta^{13}\text{C}_{\text{carb}}$ values about 1‰ that are consistent with values from the A5 Member and constrained by 4 high resolution tuff bed ages between ca. 540 Ma and 539.5 Ma (Figs. 2, 3, 5, Table S1) (Linnemann et al., 2019).

In Model A (Fig. 3b), the A4 anomaly and BACE are equivalent and constrained below the Swartpunt section in the shale interval of medium scale sequence E17 (Fig. 2). In this model, the BACE onset is at ca. 541 Ma, constrained in the A4 Member, and the recovery occurs at or before 540 Ma, constrained at the base of Swartpunt section. This is also consistent with the interpreted depositional age being close to the radiometric age determined for the sandy dolostone bed in the La Ciénega Fm, Mexico (Hodgin et al., 2020). However, this implies that 1) the clastic unit that hosts the sandy dolostone bed was deposited at a slower depositional rate above the BACE nadir, 2) the BACE recovery and plateau recorded at Swartpunt are constrained within the clastic horizon of the La Ciénega Fm and are therefore not recorded, and 3) a second more minor negative excursion is recorded above the level of the dolostone bed (possibly equivalent to the onset of 2n or a preceding minor negative excursion).

In Model A, positive $\delta^{13}\text{C}_{\text{carb}}$ values in the uppermost Spitskop Member at Swartpunt may correlate with the 2p interval in Siberia (Kouchinsky et al., 2007), Mongolia (Smith et al., 2015) and possibly Morocco (Maloof et al., 2010), all of which postdate the BACE nadir (Fig. 3b). However, in all areas that host high-resolution Fortunian $\delta^{13}\text{C}_{\text{carb}}$ records, peaks 2p-4.5p appear to be short-lived positive excursions in an interval dominated by negative mean $\delta^{13}\text{C}_{\text{carb}}$ values (Fig. 3e). The duration of the 2p interval implied by the Swartpunt radiometric data therefore appears to contradict the best-fit $\delta^{13}\text{C}_{\text{carb}}$ correlations of Fortunian sections (Maloof et al., 2010), notwithstanding the possibility for stratigraphic condensation in other regions at the 2p level (Fig. 3b and e). We consider the caveats associated with the La Ciénega Fm correlation and inconsistencies relating to inferred peak duration between Swartpunt and 2p to make Model A less likely than models B or C for the BACE position, although it remains possible.

By contrast, models B and C imply that the A4 anomaly and BACE are two distinct excursions, with nadirs that are separated from one another by up to 5 million years (Figs. 3-5). In Model B (Fig. 3c) a return to positive $\delta^{13}\text{C}_{\text{carb}}$ values following the A4 anomaly is constrained by the age of 540.095 ± 0.099 Ma at the base of the Swartpunt section, Namibia (Fig. 2) (Linnemann et al., 2019). The BACE onset occurred after ~ 539.6 Ma, as constrained by three radiometric ages from the Swartpunt section immediately below carbonates that record a decrease in $\delta^{13}\text{C}_{\text{carb}}$ to 0‰ (Figs. 2 and 3c, Table S1, Linnemann et al., 2019), which is consistent with the aforementioned radiometric constraint of 539.4 Ma from the La Ciénega Formation, Mexico (Hodgin et al., 2020). In this model, recovery from the BACE in Namibia occurred prior to ~ 538.6 Ma, consistent with a likely minimum age for the uppermost Spitskop Member at Swartpunt, as constrained by an ash bed age within the overlying Nomtsas Formation at a neighboring section (Linnemann et al., 2019) (Figs. 1 and 2). Although this model is consistent with all radiometric constraints, it implies that the BACE was a very short-lived event on the order of 1 Myr. This model demands that some sections (e.g. Sukharikha River) exhibited significantly higher sedimentation rates during the BACE (1n) interval than the overlying 2p-5p interval, which appears inconsistent with the relatively monotonous lithofacies documented throughout.

Fig. 5 presents age Model C for selected successions that host the highest resolution $\delta^{13}\text{C}_{\text{carb}}$ data for the critical late Ediacaran to Cambrian Stage 3 (Atdabanian) interval, in regions without significant Fortunian phosphorite deposition. Sections in Morocco, the Zavkhan terrane of Mongolia, and the Siberian Platform have limited Ediacaran-Fortunian radiometric ages, and therefore rely upon best-fit $\delta^{13}\text{C}_{\text{carb}}$ correlation throughout this interval. In Model C (Figs. 3d and 5), the onset of the BACE is inferred to post-date the Swartpunt section (< 538.5 Ma). Stable positive $\delta^{13}\text{C}_{\text{carb}}$ values in the interval ~ 540 – 539.5 Ma, as constrained at Swartpunt, separate the A4 anomaly from the BACE with the resulting peak herein termed the Spitskop excursion (SPIE, Figs. 3d and 5). Model C implies that 1) the A4 anomaly is distinct from the BACE, and 2) the age derived from the La Ciénega Formation (Hodgin et al., 2020) is best interpreted as detrital (Fig. 5). In this model, the sandy dolostone bed in the La Ciénega Formation was deposited up to 3 Myr after eruption of the incorporated tuffaceous material based on best fit with the $\delta^{13}\text{C}_{\text{carb}}$ curve and constant average rates of sedimentation.

Fig. 5 also shows that age-calibrated stratigraphy in many successions record a striking regional lithostratigraphic transition across the Ediacaran-Cambrian boundary interval. In many regions, the transition is marked by a widespread erosive unconformity or exposure surface (e.g. Namibia, NE Siberia), and/or a subsequent change in dominant lithofacies which may reflect changes in global sea level. Whilst invoking a eustatic driver for combined litho- and chemostratigraphic variability across this transitional interval is complicated by regional tectonics, this may have significant biostratigraphic implications that warrant future consideration.

Model C is our preferred correlation when considering best fit between sections that host continuous Fortunian $\delta^{13}\text{C}_{\text{carb}}$ data, whereby dominantly negative $\delta^{13}\text{C}_{\text{carb}}$ values are interrupted by short-lived positive excursions (Kouchinsky et al., 2007; Maloof et al., 2010) (e.g. Morocco, Siberia, Figs. 3d, e and 6). This model also permits a short-lived pre-BACE excursion (herein termed 0n) which is recorded in sections with high-resolution $\delta^{13}\text{C}_{\text{carb}}$ data from Morocco (e.g. Oued Sdas and Oued n'Oulili sections, Maloof et al., 2005), Siberia (Sukharikha and Nokhtuysk sections, Kouchinsky et al., 2007; Pelechaty, 1998), Mongolia (Zavkhan terrane, Smith et al., 2015), and possibly Laurentia (Hodgin et al., 2020; Smith et al., 2016) (Figs. 5 and 6).

Model C also maintains near constant sedimentation rates in multiple Fortunian – Stage 2 sections (Table S2). Taking two of the most continuous carbonate successions known with limited facies variation, Sukharikha River, Siberian Platform, and Zawyat n'Bougzoul, Morocco, we show that while Models A and B both show markedly declining sedimentation rates in both successions, Model C maintains a constant sedimentation rate (Fig. 6). At the resolution of lithostratigraphic detail afforded for each of these sections in the published literature, Model C appears to be the simplest and most parsimonious solution.

The maximum age for the regional FAD of *T. pedum* on the Kalahari Craton is associated with the radiometric age of the lower Nomtsas Formation, Namibia (Linnemann et al., 2019). We note, however, that *T. pedum* has not been reported from the section (Farm Swartkloofberg, Linnemann et al., 2019) from which this radiometric age is derived. Instead, the FAD of *T. pedum* is reported from entirely siliciclastic valley fill deposits of the Nomtsas Formation on Farms Sonntagsbrunn and Vergelee, >100 km to the east of Farm Swartkloofberg (Table S3). By contrast, the FAD of *T. pedum* in Laurentia is well constrained above the nadir of the BACE recorded in carbonate interbeds of the Esmeralda Member of the Deep Spring Formation, Nevada (Fig. 5c, Smith et al., 2016). If Model C is correct, then the integrated $\delta^{13}\text{C}_{\text{carb}}$ chemostratigraphy and biostratigraphy of the Mount Dunfee section may imply a far younger age for the FAD of *T. pedum* (~ 535.5 Ma), and by extension the Ediacaran-Cambrian boundary, than currently defined (Fig. 5). This may therefore also support a case for repositioning the Ediacaran-Cambrian GSSP to the Mount Dunfee section based on the best-fit calibration of the FAD of *T. pedum*.

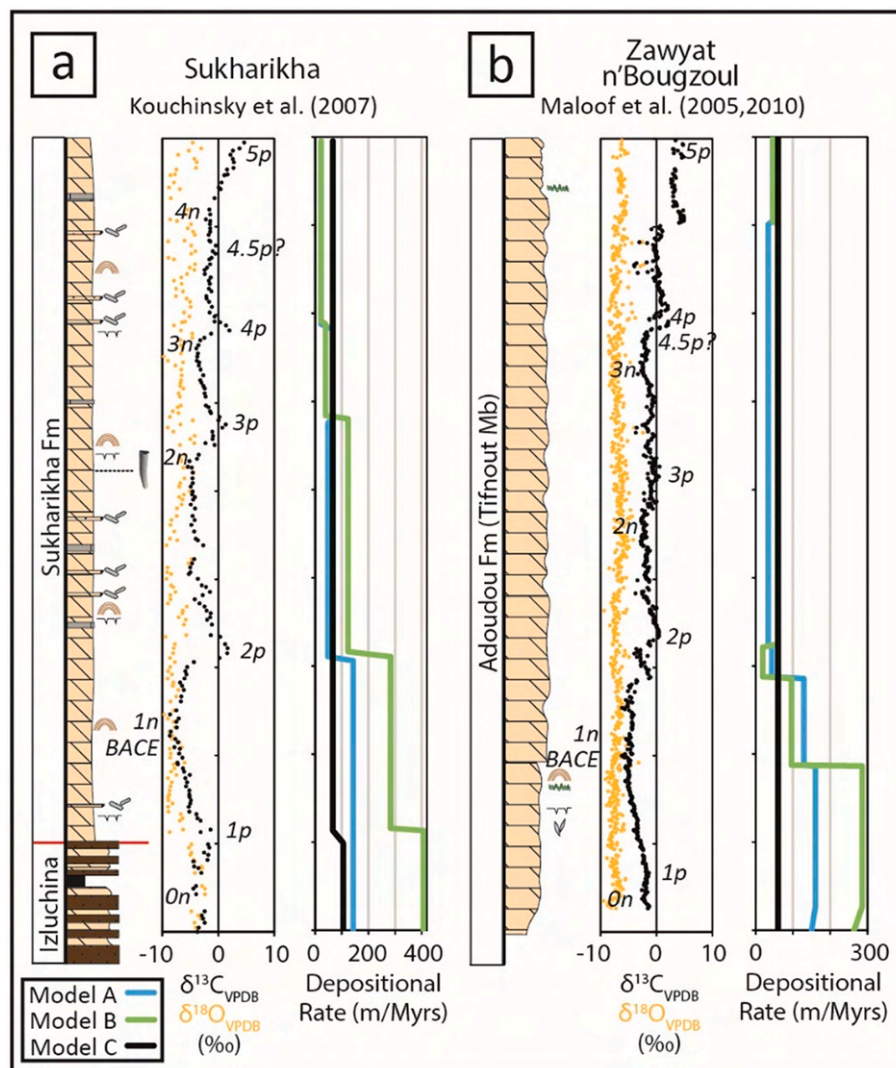


Fig. 6. Changes in sedimentation rate implied by models A to C for selected sections that capture the BACE and show limited facies variation through continuous carbonate successions. (a) Sukharikha River section (Igarka-Norilsk Uplift, Siberian Platform) and (b) Zawyat n'Bougzoul section (Anti-Atlas, Morocco), with lithostratigraphy and $\delta^{13}\text{C}_{\text{carb}}$ after Kouchinsky et al. (2007) and Maloof et al. (2005), respectively. See Fig. 2 for key to lithology and sequence stratigraphy.

5. Ongoing uncertainties and biostratigraphic constraints

The process of constructing these age models has exposed the largest remaining uncertainties in late Ediacaran – early Cambrian stratigraphic correlation, which occur mainly due to insufficient radiometric control. Despite these uncertainties, we build on the biostratigraphic framework of Maloof et al. (2010) and constrain the FADs of key Cambrian-type small skeletal fossil groups within each age model (Table S2).

5.1. The possibility for a multimodal $\delta^{13}\text{C}_{\text{carb}}$ record

High resolution $\delta^{13}\text{C}_{\text{carb}}$ and sequence stratigraphic assessment of Cryogenian and early Ediacaran carbonates of the Congo Craton has revealed significant facies-dependency in the expression of presumed-global $\delta^{13}\text{C}_{\text{carb}}$ excursions (Hoffman and Lamothe, 2019). In their model, Hoffman and Lamothe (2019) propose that the observed multimodal $\delta^{13}\text{C}_{\text{carb}}$ expression between inner platform, basin margin and upper forelope carbonates may be associated with significant facies-dependent distinction relating to seawater vs sediment-buffered diagenesis. They note that this may significantly complicate the utility of $\delta^{13}\text{C}_{\text{carb}}$ chemostratigraphic studies throughout geological time, especially where radiometric anchor-points are absent or sparse.

Anomalously positive $\delta^{13}\text{C}_{\text{carb}}$ values of the middle Bambuí Group of Brazil, stratigraphically above *Cloudina*-bearing carbonates, also clearly demonstrate offset from global seawater composition (Uhlein et al., 2019). This offset is interpreted to reflect local effects of unusual water column chemistry that likely result from partial restriction (Cui et al., 2020b; Uhlein et al., 2019).

In our models, a number of regions show a degree of scatter in $\delta^{13}\text{C}_{\text{carb}}$, with possible evidence for deviation from the idealized seawater $\delta^{13}\text{C}_{\text{carb}}$ curve. Examples include the Zuun-Arts and Salaany Gol formations (Mongolia), and potential $\delta^{13}\text{C}_{\text{carb}}$ bimodality between different facies across the Yangtze Block (South China). In particular, the negative excursions at ca. 546.5 Ma (A0) and 541 Ma (A4), which may be globally widespread, are significantly muted in sections of the Yangtze Block. Whether the excursions themselves, or the muted record in South China, best reflect true changes in seawater composition as opposed to degrees of diagenetic alteration or restriction, remains uncertain.

Resolving the possible multimodal nature of Ediacaran and lower Cambrian $\delta^{13}\text{C}_{\text{carb}}$ records will benefit from future radiometric calibration, in addition to high-resolution studies of integrated stratigraphic, petrographic, $\delta^{44/40}\text{Ca}$ and $\delta^{26}\text{Mg}$ analyses (e.g. Ahm et al., 2021; Bold et al., 2020). Whilst this frustrates the utility of the proposed global

$\delta^{13}\text{C}_{\text{carb}}$ correlation for regional chemostratigraphic studies of unfossiliferous strata with limited radiometric constraints throughout this time interval, we note that it does not alter proposed FADs and LADs of key taxa. We tentatively suggest that the broad trends observed in $\delta^{13}\text{C}_{\text{carb}}$ represented by gradual, unidirectional shifts in $\delta^{13}\text{C}_{\text{carb}}$, are consistent between sections but that the absolute magnitude of positive and negative excursions may differ depending on the specifics of local diagenetic alteration and/or steepness of the local isotopic gradient of seawater during organic carbon remineralisation. We note that this assumption holds true even for the Cryogenian interglacial interval, with the possible exception of the interval recording the Taishir anomaly (Hoffman and Lamothe, 2019). In this regard, and given the stratigraphic alternatives considered herein (Fig. 2), we do not consider the stable, positive $\delta^{13}\text{C}_{\text{carb}}$ data of the Swartpunt section to necessarily correlate with the nadir of the BACE, as has previously been suggested (e.g. Hodgin et al., 2020).

5.2. Age of the base of the Dengying Formation

In models A to C, the shape of the global composite $\delta^{13}\text{C}_{\text{carb}}$ curve between ~547 Ma and 543 Ma is dictated in large part by the age of the base of the Dengying Fm of the Yangtze Platform, South China, and the shape of the Dengying Fm $\delta^{13}\text{C}_{\text{carb}}$ profile. Detailed litho-, chemo-, and sequence stratigraphic studies of the Ediacaran Yangtze Platform are numerous (e.g. An et al., 2015; Condon et al., 2005; Cui et al., 2016b; Cui et al., 2019; Ishikawa et al., 2008; Li et al., 2013; Lu et al., 2013; Tahata et al., 2013; Wang et al., 2014, 2017; Yang et al., 2021; Zhou et al., 2017; Zhu et al., 2007, 2013). A summary description of the Dengying Fm, and detailed section correlation figures (Figs. S3 and S4) are provided herein for reference.

The Dengying Fm is lithostratigraphically subdivided into three members, each of which have differing names that correspond to geographic position on the Yangtze Platform (Fig. S3). The lower Member is dominated by dolostone that was deposited during a sea level highstand atop black shale of Member IV of the Doushantuo Formation (Zhu et al., 2007). This unit corresponds to the Algal Dolomite and Donglongtan members on the shallow Yangtze platform to the north and west, respectively, where it reaches thicknesses of >280 m. In the Yangtze Gorges area to the east, the equivalent Hamajing Member ranges in thickness from 3 to 60 m in sections measured for $\delta^{13}\text{C}_{\text{carb}}$ (Fig. S3), but may reach a maximum thickness of 200 m (Jiang et al., 2007; Zhu et al., 2007).

A sequence boundary separates dolostone of the lower Dengying Fm from overlying fossiliferous deeper marine deposits of the middle Dengying Fm across the Yangtze Platform (Zhu et al., 2007). In the north, this unit corresponds to fossiliferous transgressive siliciclastics and limestones of the Gaojiashan Member (20–45 m) (Cui et al., 2016b; Cui et al., 2019; Zhu et al., 2007). Equivalent transgressive deposits of the middle Dengying Fm correspond to shale of the Jiucheng Member (20–45 m) in the west, and bituminous limestone of the richly fossiliferous Shibantan Member (up to >100 m) in the Yangtze Gorges area to the east (Duda et al., 2016; Xiao et al., 2020; Zhu et al., 2007).

The third and topmost Member of the Dengying Fm is composed of highstand systems tract dolostones, which are frequently capped by a sequence boundary that shows evidence for exposure. In the north and west, this unit corresponds to the Beiwang (25–370 m) and Baiyanshao (≤ 120 m) members, respectively, which correlate with the Baimatuo Member (≤ 400 m) in the Yangtze Gorges area (Zhu et al., 2007). Zircons within an ash layer 45 m above the base of the Baimatuo Member at the Zhoujiaao section (central south Huangling anticline, Fig. S3) have been dated by U-Pb SIMS to 543.40 ± 3.5 Ma (Huang et al., 2020).

A zircon U-Pb CA-ID-TIMS age of 550.14 ± 0.63 Ma (Yang et al., 2021) from an ash bed at the top of Member IV (Miaohe Member) of the Doushantuo Fm at Jiuqunao section of the western Huangling anticline (Fig. S3) is classically considered to constrain a maximum age for the base of the Dengying Fm (Condon et al., 2005). The Dengying Fm in the

Jiuqunao section records recovery from a negative $\delta^{13}\text{C}_{\text{carb}}$ excursion characterised by increasing $\delta^{13}\text{C}_{\text{carb}}$ from -4.05‰ to $+3.56\text{‰}$ in <3 m of dolostone (Fig. S3) (Condon et al., 2005; Yang et al., 2021; Zhu et al., 2007). Unfortunately, lithostratigraphic and chemostratigraphic correlation between sections of the western Huangling anticline at the boundary between the Doushantuo and Dengying formations is complicated by slumping and associated stratigraphic repetition (Fig. S3) (An et al., 2015; Vernhet, 2007; Yang et al., 2021; Zhou et al., 2017). Furthermore, the ~550 Ma ash layer at Jiuqunao section has not been reported at the top of Doushantuo Member IV, or elsewhere, from any other section on the Yangtze Platform to date.

Here we consider a further alternative model (Model D) that explores the implications of correlating the $\delta^{13}\text{C}_{\text{carb}}$ data above the 550 Ma ash bed at Jiuqunao with the upper Hamajing Mb, rather than the basal Hamajing Mb (Fig. S4). In this model, the 550 Ma ash layer represents the age of slumping in the western Huangling anticline, and was deposited at the top of the disrupted unit, thereby permitting a conformable contact between the ash horizon and the overlying Dengying Fm at Jiuqunao section. The sequence stratigraphic framework for the entire Dengying Fm in sections across the Yangtze Platform and slope presented by Zhu et al. (2007) is maintained in Model D. However, this model implies that the thick Algal Dolomite and Donglongtan members, and the Hamajing Mb in many sections of the central and eastern Huangling anticline, were deposited between ≤ 565 Ma and ~550 Ma, rather than <550 Ma.

The alternative correlation presented in Model D greatly simplifies the global $\delta^{13}\text{C}_{\text{carb}}$ curve between 546 Ma and 543 Ma and, by extension, between 550 Ma and 541 Ma (Fig. 7). In models A-C, the $\delta^{13}\text{C}_{\text{carb}}$ profile from the (e.g.) Gaojiashan Member occupies the interval from 546 Ma to 543 Ma, however in Model D the middle Member of the Dengying Fm across the Yangtze Platform correlates well with the $\delta^{13}\text{C}_{\text{carb}}$ profile of the Kuibis Subgroup of the Nama Group, between 550 Ma and 546 Ma. Model D also implies that the Aim and Khatyspyt formations of the Siberian Platform may similarly occupy the interval from 550 Ma to 546 Ma based on best fit with the resulting global $\delta^{13}\text{C}_{\text{carb}}$ curve (Fig. 7d). In Model D, the global $\delta^{13}\text{C}_{\text{carb}}$ curve between 546.5 Ma and 541 Ma is characterised by a simple increase and decrease (Fig. 7b), from A0 to A3 and culminating in the A4 excursion (which may or may not correspond with the BACE).

5.3. Age of the Khatyspyt Formation

The temporal placement of the Khatyspyt Formation of the Olenek Uplift is key to understanding the degree of assemblage overlap between the Avalon, White Sea and Nama assemblages, as it contains typical Avalon assemblage fossils including the rangeomorphs *Charnia masoni* and *Khatyspytia grandis* (e.g. Cui et al., 2016a). The age of the Khatyspyt Formation also has significant implications for the evolution and morphological changes in macroalgae during the late Ediacaran (Bykova et al., 2020). The Khatyspyt Formation has long been assumed to record deposition between ca. 560 and 550 Ma, approximately contemporaneously with the Miaohe Member (South China) and fossiliferous deposits of the White Sea area (e.g. Cui et al., 2016a). In fact, the only radiometric constraint available is a maximum age for intrusion of the volcanic breccia of the Tas-Yuryakh volcanic complex within the lower part of the Syhargalakh Formation (lower Kessyusa Group), which unconformably overlies the Khatyspyt and overlying Turkut formations. The maximum age for intrusion of this unit is 542.8 ± 1.30 Ma, provided by zircon U-Pb air abrasion ID-TIMS (Table S1) (Bowring et al., 1993; Maloof et al., 2010; Rogov et al., 2015). Notwithstanding uncertainties in this age (Table S1), the Turkut Formation, which overlies the Khatyspyt Formation, contains the local FAD of the anabaritid *Cambrorhabdus decurvatus* and the onset of a negative excursion which may be equivalent either to the A4 anomaly or the BACE (depending on the preferred model, Figs. 3 and 4). Screened $^{87}\text{Sr}/^{86}\text{Sr}$ data for the Khatyspyt Formation (boxed data in Fig. 4b-d) are notably depleted (mean =

constrained sections (e.g. Ara Group, Oman, Amthor et al., 2003; Bowring et al., 2007). Robust $^{87}\text{Sr}/^{86}\text{Sr}$ data from the Nama Group are recorded from samples spanning the Omkyk Member (Zaris Formation) to the Nomtsas Formation, with relatively invariable $^{87}\text{Sr}/^{86}\text{Sr}$ values (mean = 0.708538, $n = 11$) (Kaufman et al., 1993). Furthermore, high Sr limestones from the Shibantan Member, South China and the Zuun-Arts and overlying Bayan-Gol formations of the Zavkhan Terrane, Mongolia, show robust $^{87}\text{Sr}/^{86}\text{Sr}$ values and $\delta^{13}\text{C}_{\text{carb}}$ trends consistent with the record from the Nama Group, with the latter extending relatively stable values of ~ 0.708500 into the lower Fortunian (Fig. 4b-d, Table S2, Brasier et al., 1996). In light of available robust $\delta^{13}\text{C}_{\text{carb}}$ and $^{87}\text{Sr}/^{86}\text{Sr}$ data from radiometrically well-constrained sections, our compilation suggests either: 1) that low $^{87}\text{Sr}/^{86}\text{Sr}$ values and an Avalon-type biotic assemblage support an older temporal placement for the Khatyspyt Formation than that shown in our compilation (>551 Ma and possibly as old as ~ 575 Ma), or 2) that the $^{87}\text{Sr}/^{86}\text{Sr}$ data recorded by the Khatyspyt Formation are not representative of global seawater composition. The nature of the contact between the Khatyspyt and Turkut formations along the Khorbusuonka River is key to determining the true placement of the Khatyspyt Formation, and reports vary considerably. For example, Cui et al., 2016a report that the boundary between the Khatyspyt and Turkut formations is conformable, whereas Vishnevskaya et al. (2017) suggest that this is an unconformable contact. However, neither publication provides figured evidence of the nature of the contact.

In our correlation, we tentatively assume that the hiatus (if any) at the boundary between these two formations along the Khorbusuonka River is relatively minor (<500 kyrs). This is justified in part by the consistency in $\delta^{13}\text{C}_{\text{carb}}$ and lithostratigraphy between late Ediacaran sections of the Olenek uplift and the Nama and Ara groups (Figs. 3 and 5). However, we stress that this requires future clarification due to the unusually low $^{87}\text{Sr}/^{86}\text{Sr}$ data of the Khatyspyt Formation in this time interval. If the boundary is conformable, the presence of Avalon-type fossils in the Khatyspyt Formation, in addition to *Charniodiscus* noted from the Shibantan Member (Chen et al., 2014), together suggest that rare remnants of the Avalon assemblage remained until possibly as late as ca. 545.5 Ma. It is noteworthy that ordination plots of the overall late Ediacaran fossil assemblages have not placed the Khatyspyt assemblage within the Avalon-type biotas and instead place it with the younger White Sea biota (Boag et al., 2016). The temporal overlap between the Avalon and Nama assemblages also holds true regardless of the age of the Khatyspyt Formation, as the age of the Shibantan Member is confidently constrained ($< \text{ca. } 551$ Ma) by the aforementioned radiometric age of the volcanic tuff deposit in the underlying upper Miaohu Member (Condon et al., 2005; Schmitz, 2012; Yang et al., 2021).

5.4. Age of the Turkut Formation

A maximum age for intrusion of the Tas-Yuryakh volcanic breccia within the lower Syhargalakh Formation (lower Kessyusa Group) along the Khorbusuonka River is suggested by a zircon U-Pb air abrasion ID-TIMS age of 542.8 ± 1.30 Ma (Table S1) (Bowring et al., 1993; Maloof et al., 2010; Rogov et al., 2015). The intrusive Tas-Yuryakh volcanic breccia unconformably overlies the Turkut Formation. The FAD of the anabaritid *Cambrotubulus decurvatus* is recorded from the lower Turkut Formation in this section (Rogov et al., 2015), which supports a late Ediacaran lower boundary for the regional Nemakit-Daldynian Stage of Siberia, consistent with biostratigraphy and $\delta^{13}\text{C}_{\text{carb}}$ chemostratigraphy in sections along the Yudoma River of SE Siberia (Zhu et al., 2017). $\delta^{13}\text{C}_{\text{carb}}$ chemostratigraphic and sequence stratigraphic studies support temporal placement of the Turkut Formation of the Khorbusuonka River correlative with the middle – upper Ust'-Yudoma Formation in sections along the Yudoma River (Knoll et al., 1995; Pelechaty, 1998; Pelechaty et al., 1996b; Pelechaty et al., 1996a; Zhu et al., 2017). Indeed, if the age of the Tas-Yuryakh volcanic breccia is close to the minimum age within analytical uncertainty, then the negative excursion recorded at the top of the Turkut Formation (Knoll et al., 1995) is equivalent to the A4

anomaly, and either corresponds with (Model A) or precedes (models B and C) the BACE. In both scenarios, the lower Turkut Formation and middle Ust'-Yudoma Formation at Kyra-Ytyga contain the earliest known FADs of anabaritids globally (≥ 541 Ma, Fig. 8). It is likely that future high precision CA-ID-TIMS analyses significantly alter the temporal position of the Tas-Yuryakh volcanic breccia, and by extension the minimum age of the underlying Turkut Formation. In the age models presented herein, a maximum age for the FAD of SSFs of the *Anabarites trisulcatus* – *Protohertzina anabarica* Zone (and by extension the Nemakit-Daldynian lower boundary) is therefore set at ca. 541–542 Ma across the Siberian Platform (Fig. 8). This temporal placement is most consistent with the dominant $\delta^{13}\text{C}_{\text{carb}}$ trends observed pre-BACE, whereby positive $\delta^{13}\text{C}_{\text{carb}}$ values are interrupted by short-lived negative excursions (Fig. 3e).

5.5. Integrated geochronology of the Ara Group

A complication inherent in the chemostratigraphic assessment of the Ara Group is the nature of the carbonate units themselves, which are found as 'stringers', frequently interbedded by evaporite (Amthor et al., 2003; Bowring et al., 2007). We note that whilst the high precision radiometric ages provided by Bowring et al. (2007) confidently place these carbonate units in relative stratigraphic order, the analyzed tuffaceous material and $\delta^{13}\text{C}_{\text{carb}}$ datasets do not always derive from the same core. For example, the A0 $\delta^{13}\text{C}_{\text{carb}}$ excursion is recorded within the Sabsab-1 well, whereas the radiometric constraint of ~ 546.72 Ma derives from a tuff bed in the Asala-1 well. $\delta^{13}\text{C}_{\text{carb}}$ data for the Asala-1 well remain unpublished, precluding confident calibration of this $\delta^{13}\text{C}_{\text{carb}}$ excursion. Indeed, the only two wells for which both radiometric and $\delta^{13}\text{C}_{\text{carb}}$ data are available are BB-5 and Minha-1. Whilst BB-5 constrains the A4 anomaly, Minha-1 captures positive $\delta^{13}\text{C}_{\text{carb}}$ values in the A3 Member that are in agreement with radiometrically constrained $\delta^{13}\text{C}_{\text{carb}}$ data from Brazil (Parry et al., 2017) and South China (Huang et al., 2020).

We note that some other globally-distributed sections record an excursion that is demonstrably pre-BACE (e.g. Zuun-Arts Formation), which may be more consistent with an earlier, distinct 'A4' anomaly. The A5 Member of the Ara Group also records a $\delta^{13}\text{C}_{\text{carb}}$ plateau of similar magnitude to that recorded at Swartpunt (Fig. 5a, b), followed by a gradual decrease in $\delta^{13}\text{C}_{\text{carb}}$ that mirrors the decrease seen above the level of the ca. 539.6 Ma horizon at Swartpunt (Figs. 2 and 5a, b). These features may add credence to a pre-BACE 'A4' anomaly (models B and C).

5.6. $\delta^{13}\text{C}_{\text{carb}}$ correlation of the lower Fortunian

Recent biostratigraphic and $\delta^{13}\text{C}_{\text{carb}}$ chemostratigraphic assessment of Ediacaran – Cambrian transitional strata of the Yangtze Platform, South China have shown a previously underappreciated level of $\delta^{13}\text{C}_{\text{carb}}$ variability in the post-BACE, pre-ZHUCE (Zhujiqing positive $\delta^{13}\text{C}_{\text{carb}}$ excursion) interval (Steiner et al., 2020). In age models A and B, the BACE is constrained to be late Ediacaran in age, with a nadir either at ca. 541 (Model A) or ca. 539 Ma (Model B, Figs. 3 and 9, Table S2). In Model C, the BACE is within the basal Cambrian based on correlation with the radiometric age and inferred maximum FAD of *T. pedum* in the Nomtsas Fm (Fig. 10). However, as noted above, the FAD of *T. pedum* is constrained to be post-BACE in all successions that host the BACE, which may also support an Ediacaran age for the BACE in Model C. The BACE is well-recorded in sections across the Yangtze Platform, South China, in the lower Zhujiqing Formation (Daibu Member) and Yanjiahe Formation, and is commonly overlain by phosphorus-rich carbonates of the middle Zhujiqing Formation (Zhongyicun Member) and equivalent units (Brasier et al., 1990; Steiner et al., 2020). Phosphorite deposition is globally widespread in lower Fortunian strata (e.g. Tarim, Yangtze Platform, Malyi Karatau of Kazakhstan, northern Mongolia, some sections of Laurentia), with carbonate substituted in the phosphorite lattice

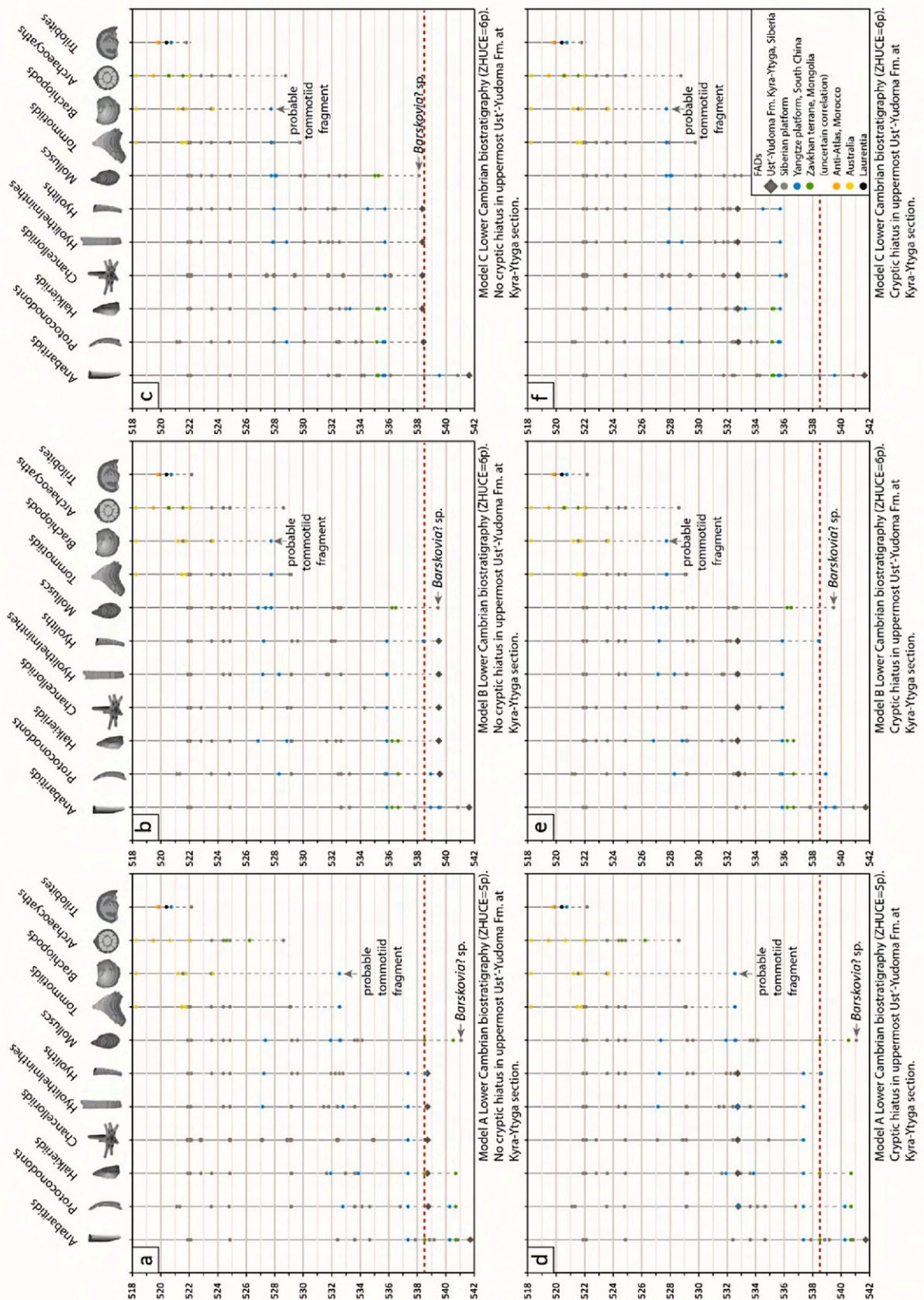
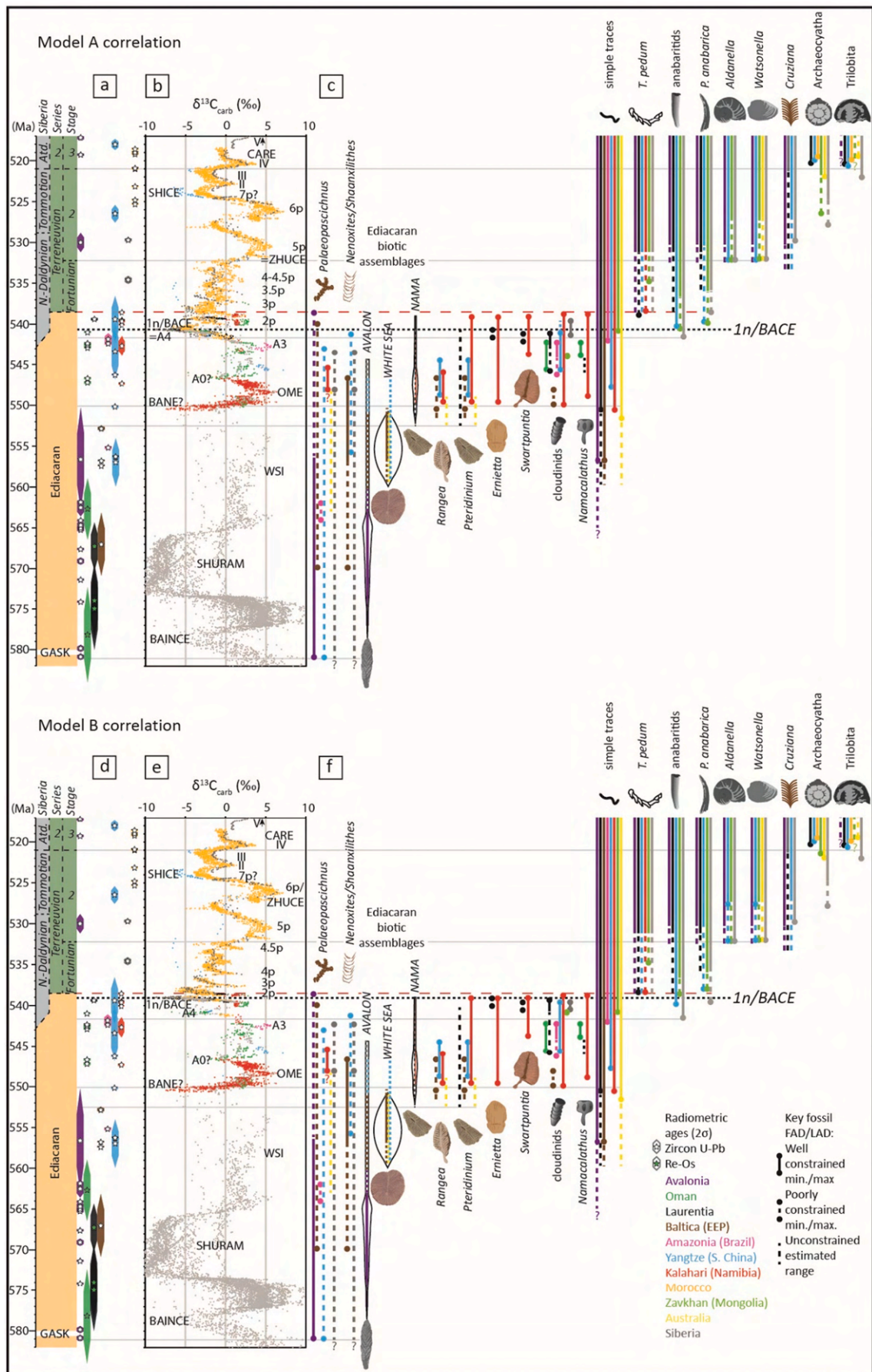


Fig. 8. High-resolution Cambrian biostratigraphy resulting from models A to C. Note that first occurrences are pinned only within sections that have high-resolution $\delta^{13}\text{C}_{\text{carb}}$ data. As such, first appearances within siliciclastic-dominated successions remain uncalibrated. The single specimen of *Aldanotreta* sp. (brachiopod) reported from the upper Zhongyicun Member (Table S2) may instead represent a tommotiid fragment; however, this cannot be confirmed due to the poor quality of the specimen.



(caption on next page)

Fig. 9. Biostratigraphic output resulting from Model A (a–c) and Model B (d–f) for the interval ~ 551–517 Ma. Includes (a,d) radiometric constraints, (b,e) $\delta^{13}\text{C}_{\text{carb}}$, and (c,f) First Appearance Datum (FAD) and Last Appearance Datum (LAD) of key Ediacaran-Cambrian fossils (Table S3). Black dotted line marks the temporal position of the 1n/BACE nadir. Red dashed line marks the Ediacaran-Cambrian boundary as defined by the maximum age for the first appearance datum of *Treptichnus pedum*. Note that uncertainty remains in ichnofossil assignment of the traces in the Mistaken Point Formation of Avalonia (Warren et al., 2020). (For interpretation of the references to colour in this figure legend, the reader is referred to the web version of this article.)

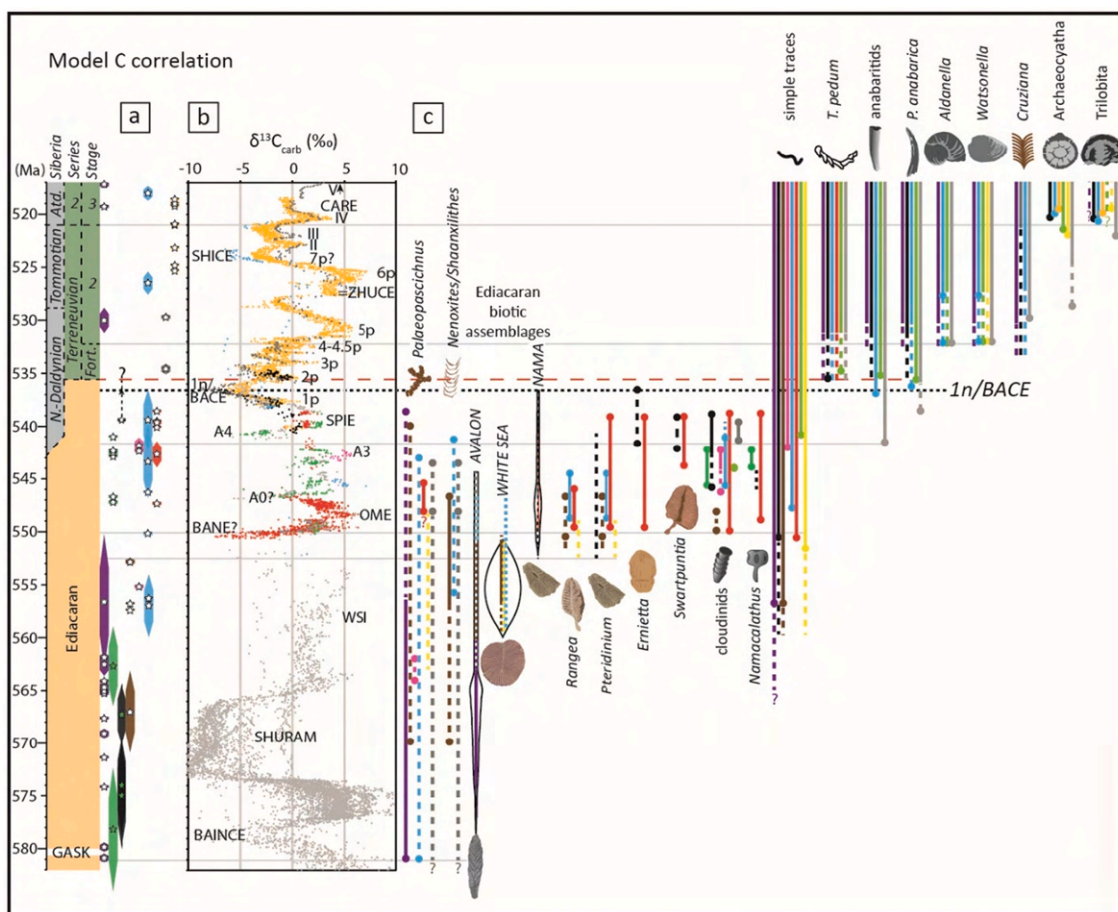


Fig. 10. Biostratigraphic output resulting from Model C (a–c) for the interval ~ 551–517 Ma. Includes (a) radiometric constraints, (b) $\delta^{13}\text{C}_{\text{carb}}$, and (c) First Appearance Datum (FAD) and Last Appearance Datum (LAD) of key Ediacaran-Cambrian fossils (Table S3). Black dotted line marks the temporal position of the 1n/BACE nadir. Red dashed line marks the Ediacaran-Cambrian boundary as defined by the maximum age for the first appearance datum of *Treptichnus pedum*. In this figure, the FAD of *T. pedum* is interpreted to post-date the BACE nadir in all regions (max. FAD in upper Esmeralda Mb, Nevada, Fig. 5c), and the age of the lower Nomsas Fm at Swartkloofberg section does not anchor the FAD of *T. pedum* in Namibia (see discussion in Section 4). Key provided in Fig. 9. (For interpretation of the references to colour in this figure legend, the reader is referred to the web version of this article.)

commonly recording very negative, or highly variable $\delta^{13}\text{C}_{\text{carb}}$ values that diverge from global seawater composition. The upper Yanjiahe Formation, above the level of the BACE, yields highly variable $\delta^{13}\text{C}_{\text{carb}}$ values alongside SSFs of the *A. trisulcatus* – *P. anabarica* assemblage Zone (Steiner et al., 2020). The Kuanchuanpu Formation yields similarly variable $\delta^{13}\text{C}_{\text{carb}}$ values and SSFs (Steiner et al., 2020; Yang et al., 2016b). Crucially, the lower Kuanchuanpu Formation records the co-occurrence of *Cloudina* with SSFs of the *A. trisulcatus* – *P. anabarica* Zone (Yang et al., 2016b), however the exact position of this mixed assemblage relative to the BACE nadir remains uncertain.

In areas where phosphorite deposition is limited, the $\delta^{13}\text{C}_{\text{carb}}$ composition of Fortunian-age global seawater is more faithfully recorded (e.g. Siberia, Morocco, Mongolia), and appears to show high frequency excursions (including peaks 2p–4p) that record a gradual increase in $\delta^{13}\text{C}_{\text{carb}}$ towards a large positive excursion (5p) (Figs. 3b–d, 5d–f) (Kouchinsky et al., 2007; Maloof et al., 2010; Smith et al., 2015). Crucially, however, this interval of high frequency $\delta^{13}\text{C}_{\text{carb}}$ variability suffers from a significant dearth of radiometric anchor-points, robust

differentiation in SSF zonation, or differentiation of $\delta^{13}\text{C}_{\text{carb}}$ peaks of distinct magnitude. Sections of the Anti-Atlas Mountains in Morocco and along the Sukharikha River of northwest Siberia have been proposed as continuous reference sections for correlative trends in Fortunian global seawater $\delta^{13}\text{C}$ (Kouchinsky et al., 2007; Maloof et al., 2010). However, the absolute magnitude and number of peaks are thought to vary between and within regions (e.g. Smith et al., 2015). At present, the published section information in both of these areas is insufficiently detailed to accurately constrain the position of individual exposure surfaces. We note that the Fortunian remains the interval of greatest uncertainty in our correlation and demands future targeted study, integrating high resolution chemostratigraphic data with detailed sedimentological, biostratigraphic and sequence stratigraphic information and, where possible, high resolution radiometric age constraints. Higher resolution $\delta^{13}\text{C}_{\text{carb}}$ datasets may also permit more statistically significant peak correlation through use of dynamic programming algorithms, as has been demonstrated for Atdabanian successions of Morocco (Hay et al., 2019).

5.7. The position of the ZHUCE relative to peaks 5p and 6p

Below we consider alternative temporal positions for the ZHUCE and the excursion recorded in the Salaany Gol Formation. For ease of reference, alternative correlations are incorporated into Model A relative to models B and C, however their relative positions and uncertainties should be considered in isolation.

The upper Zhujiqing Formation (Dahai Member) of the Yangtze Platform records a prominent positive $\delta^{13}\text{C}_{\text{carb}}$ excursion with an onset approximately coincident with the FADs of the mollusks *Aldanella attleboensis* and *Watsonella crosbyi* (Figs. 8–10, Table S3, Li et al., 2011; Parkhaev and Karlova, 2011; Steiner et al., 2020). The FAD of *Watsonella crosbyi* occurs prior to the apex of 5p, or immediately following recovery from 5p in sections of the western Anabar Shield, and may be approximately contemporaneous in the Bayangol Fm of the Zavkhan Terrane, Mongolia (Kouchinsky et al., 2017; Smith et al., 2015) (but see section 5.8). Peak 5p is followed by 6p in Cambrian Stage 2 strata of Siberia and Morocco, but the relative position of the singular excursion recorded in the Dahai Member has been problematic (Steiner et al., 2020). Possible regional variability in the magnitude of the ZHUCE in South China, in addition to widespread phosphorite deposition of the underlying Zhongyicun Member in some areas of the Yangtze Platform, complicates the utility of $\delta^{13}\text{C}_{\text{carb}}$ chemostratigraphy for accurately determining the correct correlation of the peak recorded in the Dahai Member (Steiner et al., 2020).

Model A (Figs. 3b, 8a, 9b,c) shows the result of correlating the ZHUCE with 5p, which may be more consistent with a depositional hiatus of longer duration that separates the Dahai Member from the overlying Shiyantou Formation. In this correlation, the FAD of tommotiids in South China significantly predates Siberia (Fig. 8a), and maximum $\delta^{13}\text{C}_{\text{carb}}$ values of the Dahai Member are greater than 5p in the Siberian and Moroccan profiles. However, Model A results in a relatively consistent (possibly slightly earlier) FAD of the mollusks *Watsonella* and *Aldanella* in South China relative to Siberia (Fig. 9c), whereas Model B results in a slightly delayed FAD of these genera in South China (Figs. 8b and 9f). Correlation of the ZHUCE with 5p is also supported by SSF biostratigraphy of the Yanjiahe Fm, where peak values in Unit 3 occur within the SSF Zone 2 (*Purella antiqua*), which would be consistent with a pre-5p excursion in other localities.

In models B and C, the ZHUCE is correlated with peak 6p (Figs. 3c,d, 8b,c, 9f, 10c) and negative $\delta^{13}\text{C}_{\text{carb}}$ values associated with phosphatic lithologies of the Zhongyicun Member are not considered useful for global chemostratigraphic correlation. Correlation of the ZHUCE with 6p may be justified by the best fit of $\delta^{13}\text{C}_{\text{carb}}$ data (particularly maximum values at Xiaotan section), but also by recognition of the more consistent age for the resulting FAD of tommotiids in South China relative to Siberia (Fig. 8b,c). In Model B, positive $\delta^{13}\text{C}_{\text{carb}}$ in Yanjiahe Unit 3 are correlated with peak 5p, and peak 6p is absent from this formation in recognition of the depositional hiatus separating the Yanjiahe Formation from the overlying Shuijingtuo Formation (Steiner et al., 2020). Robust differentiation between these correlations is currently hampered by a lack of radiometric data and discontinuous carbonate sections from this interval in South China.

5.8. Correlation of the Salaany Gol Formation (Zavkhan Terrane, Mongolia) with peak 6p vs peak IV

A basal Tommotian (Stage 2) age for the lower Salaany Gol (Salaany) Formation of SW Mongolia was justified by Smith et al. (2015) on the basis of an absence of trilobites in this unit, which in their view makes the excursion equivalent to positive peak 6p of the Siberian scale (shown in Model A of Figs. 3a, 8a, 9b). However, the archaeocyathan assemblage of the lower Salaany Gol Formation includes approximately 30 distinct species (up to 16 species per single reef; Zhuravlev and Naimark, 2005), which are widespread throughout Mongolian, Altay-Sayan and Transbaikalian terranes and occur permanently below the

first trilobites in each area (Debrenne et al., 2015; Dyatlova and Sycheva, 1999; Osadchaya and Kotel'nikov, 1998; Zhuravleva et al., 1997). In turn, this first trilobite species assemblage is also the same and belongs to the *Resimopsis* trilobite Zone, which contains species of the middle Atdabanian (Stage 3) *Repinaella* trilobite Zone of the Siberian Platform and lacks any earlier trilobite elements (Astashkin et al., 1995; Korobov, 1989; Korobov, 1980). Landing and Kruse (2017) noted these inconsistencies and suggested that the positive $\delta^{13}\text{C}_{\text{carb}}$ excursion in the lower Salaany Gol Formation is rather an equivalent of the middle Atdabanian $\delta^{13}\text{C}_{\text{carb}}$ excursion IV of the Siberian Platform, which fits better to both archaeocyath and trilobite biostratigraphies. The other suggestion of Smith et al. (2015) concerning the absence of upper Atdabanian and Botoman (stages 3 and 4) faunal elements from the Salaany Gol Formation is correct and supported by the restudy of archaeocyath species assemblage, which is the same through the entire formation (Cordie et al., 2019; Debrenne et al., 2015; Zhuravlev, 1998).

We agree with Smith et al. (2015) that the magnitude of the positive $\delta^{13}\text{C}_{\text{carb}}$ excursion reported from the Salaany Gol Formation fits well with peak 6p on the reference scale, but greatly exceeds the magnitude of peak IV (Figs. 3, 5f, Table S2). However, we also note that the regional $\delta^{13}\text{C}_{\text{carb}}$ record from the Zavkhan terrane throughout the underlying Zuun-Arts and Bayangol formations frequently exhibits more extreme values (positive and negative) relative to other late Ediacaran and lower Cambrian records from Siberia, Morocco and elsewhere. Models B and C (Figs. 3c,d, 8b,c, 9e,f, 10b,c) reposition the Salaany Gol Formation to the Atdabanian, with the uppermost Bayan Gol Formation occupying a position relative to peak 6p, and imply poor expression of peak 5p, possibly within lower Member BG5 of Smith et al. (2015) (Fig. 5f). We stress, however, that peak correlation throughout the Fortunian and Stage 2 of Mongolia, and globally, remains poorly constrained.

5.9. Age and correlation of Terreneuvian – Series 2 strata of Australia

The Arrowie and Stansbury basins contain a rich assemblage of lower Cambrian fossils, including the regional first appearance of archaeocyaths, trilobites, bradoriids and tommotiids. Betts et al. (2019, 2018, 2017a, 2017b, 2016) and Jago et al. (2020) refined the lower Cambrian biostratigraphy for South Australia developed by Daily (1990, 1972), Laurie (1986), Gravestock (1984), Bengtson et al. (1990), Zhuravlev and Gravestock (1994), and Gravestock et al. (2001) and added $\delta^{13}\text{C}_{\text{carb}}$ chemostratigraphy. Contrary to previous workers, Betts et al. (2019, 2018, 2017a, 2017b, 2016) and Jago et al. (2020) suggested that lower units of fossiliferous strata of the Arrowie and Stansbury basins be repositioned to stages 2 and 3 instead of stages 3 and 4, respectively. These justifications were mostly based on tommotioid biostratigraphy, with little reference to other biostratigraphic constraints. However, Australian tommotiids are highly endemic species and some genera are unknown even beyond the Australian-Antarctic faunal province of Gondwana, while other faunal elements, including archaeocyaths, trilobites, bradoriids, mollusks and brachiopods are much more widespread, although at the generic level (Bengtson et al., 1990; Betts et al., 2017b; Brock et al., 2000; Gravestock et al., 2001; Laurie, 1986). In dismissing the biostratigraphic value of archaeocyaths, for instance, these authors arrive at a correlation of their *Kulparina rostrata* tommotioid Zone and the regionally pre-trilobitic portion of their succeeding *Micrina etheridgei* Zone with the Cambrian Stage 2, even though these zones collectively coincide with the *Warriootacyathus wilkawillinensis*, *Spirilicyathus tenuis* and *Jugalicyathus tardus* archaeocyath zones (Zhuravlev and Gravestock, 1994), dated as Atdabanian in Siberian terms (Stage 3). Likewise, comparison of archaeocyath genera in common with South China indicates a correlation with trilobite-bearing upper Qiongzhusian-lower Canglangpuan (Stage 3) strata in that region (Yang et al., 2016a). The same conclusions contradicting the correlations of Betts et al. (2018, 2017a) follow from analysis of the biostratigraphic distribution of any other fossil group present in these tommotioid-based zones, including bradoriids, brachiopods (Kruse et al., 2017) and

mollusks (Parkhaev, 2019). In general, tommotiids and coeval early small shelly fossils in South Australia are not indicative of the Terreneuvian because representatives of all other co-occurring fossil groups (archaeocyaths, bradoriids, brachiopods, mollusks) are restricted to post-Terreneuvian strata in Siberia, South China, Laurentia and other regions, and more precisely to global stages 3 and 4 (Kruse et al., 2017; Parkhaev, 2019), which suggests different, younger ages for some of the $\delta^{13}\text{C}_{\text{carb}}$ peaks, rather than those accepted by Betts et al. (2018). In our correlation, we have repositioned some of these Australian $\delta^{13}\text{C}_{\text{carb}}$ data to maintain consistency with both the regional stratigraphic correlation of Betts et al. (2018) and biostratigraphic constraints that are more globally applicable (Figs. 9 and 10, Table S2).

6. Implications for macroevolutionary dynamics

Our revised correlations have important implications both for the late Ediacaran global $\delta^{13}\text{C}_{\text{carb}}$ profile and for macroevolutionary dynamics across the BACE interval. Combining the temporal and spatial distribution of major Ediacaran-Cambrian shelly and trace fossils into these new global $\delta^{13}\text{C}_{\text{carb}}$, $^{87}\text{Sr}/^{86}\text{Sr}$ and geochronological records, together with older Ediacaran radiometric dates, allows us to establish temporal and spatial paleobiogeographic trends that significantly diverge from the accepted consensus (Figs. 8-11; Table S3). These trends are robust despite remaining uncertainties, and crucially, all age models show the same macroevolutionary trends across the Ediacaran-Cambrian boundary interval (Figs. 8-10). Namely, that multiple negative $\delta^{13}\text{C}_{\text{carb}}$ excursions are present in the late Ediacaran record, which do not clearly correlate with extinction events and that SSFs of the *A. trisulcatus* – *P. anabarica* Zone appeared below the BACE.

The available radiometric age constraints for the interval of ~580–538 Ma confirm the temporal overlap of elements of the Avalon, White Sea and Nama assemblages of the Ediacaran biota, rather than forming discrete successive assemblages, with the White Sea assemblage being entirely transitional (Grazhdankin, 2014; Yang et al., 2021). Consistent with previous models, the Ediacaran biota show a marked decline in diversity ~550 Ma, and again ~545 Ma (Boag et al., 2016; Grazhdankin, 2014; Muscente et al., 2019). Elements of the Avalon and White Sea assemblages inhabited different basins contemporaneously in the White Sea and Podolia regions of Baltica, and Australia, until ~552 Ma (Gehling and Droser, 2013; Grazhdankin, 2014), although the age range of fossiliferous strata of the Ediacara Member remains poorly constrained. Both the Avalon and White Sea assemblages largely disappeared by ~550 Ma, however some elements of the Avalon assemblage (e.g. *Charniodiscus*) and White Sea assemblage (e.g. possible *Dickinsonia* sp.) were likely present until as late as ~545.5 Ma in South China and possibly northern Siberia (e.g. Cui et al., 2016a; Xiao et al., 2020). After this time, taxa of the Nama assemblage remained present in the Nama Basin, Namibia, the Erga Formation of the White Sea region, the Shibantan Member of the Yangtze Block, South China, and the Wood Canyon Formation of Laurentia. Successions of Armorica (Spain) and SW Gondwana (Brazil and Paraguay) also host skeletal assemblages of *Cloudina*, *Namacalathus* and *Corumbella* (Adorno et al., 2017; Cortijo et al., 2010; Warren et al., 2011), however these successions remain poorly constrained in time < 550 Ma due to a dearth of high resolution $\delta^{13}\text{C}_{\text{carb}}$ data. Fossils of the *Palaeopascichnus* group may have extended below ~560 Ma in the Shuram-Wonoka negative excursion interval in South Australia. However, these taxa are known from ~547–545 Ma in Siberia (Aim Formation), South China (Gaojiashan and Shibantan members, and Liuchapo Formation) and Namibia (Schwarzrand Subgroup), and may show their greatest range in eastern Newfoundland, where they are found below a Gaskiers age diamictite (>580 Ma) and even co-occur with *T. pedum* above the basal Cambrian GSSP (Table S3).

Treptichnid trace fossils pre-date the inferred nadir of the BACE in Namibia, and Cambrian-type shelly fossils of the *Anabarites trisulcatus* – *Protohertzina anabarica* Zone predate the nadir of the BACE in Siberia and predate or co-occur with the nadir of the BACE in South China (Cai

et al., 2019; Jensen et al., 2000; Zhu et al., 2017). Diverse and complex ichnofossils also predate the *T. pedum* FAD in a number of sections (e.g. Chen et al., 2019; Gozalo et al., 2003; Jensen et al., 2000; Zhu et al., 2017). At least three soft-bodied genera of the Nama assemblage are present in the Nama Basin, Namibia, post-dating (Model A), coeval with (Model B), or pre-dating (Model C) the inferred position of the BACE, and both *Cloudina* and *Namacalathus* occur above the inferred recovery from the A4 anomaly in the same section in all models (Fig. 2, Darroch et al., 2015; Narbonne et al., 1997; Wood et al., 2015). There are currently no environments that show unequivocal co-occurrence of the Cambrian ichnospecies *T. pedum* and Ediacaran skeletal fossils *Cloudina* or *Namacalathus*. These taxa, as well as *Nenoxites* (= *Shaanxilithes* in South China) became extinct at or before the Ediacaran-Cambrian boundary, as defined by the FAD of *T. pedum*, but significantly these extinctions were regional, rather than global events (e.g. *Cloudina* LAD may be as early as ~542.3 Ma in Oman (Bowring et al., 2007), but occurred after ~539.6 Ma in Namibia (Linnemann et al., 2019)).

Model C may support a range extension for erniettomorphs in Laurentia associated with the BACE nadir, to an age that is within the lower Cambrian as presently defined (Figs. 5 and 10). However, Model C may also imply a younger age for the FAD of *T. pedum* (and hence the Ediacaran-Cambrian boundary) if this ichnospecies is restricted to a position above the BACE recovery as suggested in multiple regions (Figs. 5 and 10, Table S3). The *T. pedum* FAD may show broadly synchronous origination at the boundary above recovery from the BACE, with a maximum radiometric age constraint of ~538.8 Ma (Linnemann et al., 2019). However, the first appearance of this ichnospecies is delayed in the Zavkhan terrane, and is not well constrained within the interval 538.8–532 Ma in Siberia, South China or the lower Cambrian boundary type section in Avalonia (Table S3). This pattern may be a consequence of local ecological, taphonomic and/or lithological controls.

The FADs of Ediacaran and Cambrian shelly fossils are also highly variable temporally and spatially (Figs. 8-10). The *Cloudina* – *Namacalathus* assemblage appeared ~550 Ma in the Nama Basin and became globally widespread, but asynchronously, thereafter. *Anabarites trisulcatus* and *Protohertzina anabarica* FADs, which are commonly recognized as the index fossils of the basal Cambrian strata, are in fact oldest in Siberia, where *Anabarites* co-occurs with *Cloudina* at a level below the BACE (Figs. 8-10) (Zhu et al., 2017), followed closely by the appearance of these taxa in South China (Cai et al., 2019). Cambrian-type skeletal fossils (halkieriids, chancelloriids, hyolithelminthes, hyoliths, archaeocyaths and many others) also appear highly asynchronously in different basins (Fig. 8).

By contrast, our compilation suggests that the appearance of *Watsonella* and *Aldanella* at ~532–531 Ma may have had a broadly synchronous appearance during the same interval on the global $\delta^{13}\text{C}_{\text{carb}}$ profile, however this remains dependent upon the correlation of the ZHUCE in South China (Figs. 8-10). The probability of a trilobite biomineralisation event at ~521–518 Ma is supported by the stratigraphic and paleogeographic distribution of arthropod scratch marks (e.g. *Rusophycus*, *Cruziana* and *Diplichnites*), which occur from ~531–525 Ma and pre-date the appearance of trilobites and other arthropods in almost every basin by several million years (Landing et al., 2020; Paterson et al., 2019). This biomineralisation event may have been driven by changing seawater chemistry (e.g. Mg/Ca ratios, $p\text{CO}_2$), causing a shift from aragonite to calcite seas (Porter, 2007).

These observations may imply two patterns of first appearance. In the first case, an animal or a group of animals appeared first in a single area and became globally widespread much later (e.g. Namibian shelly fossils including *Cloudina* and *Namacalathus*, Siberian archaeocyaths). The appearance of such organisms probably reflects local conditions most advantageous for their oxygen, calcium and other essential requirements. The second type of FADs embraces a broadly synchronous global appearance of the same group in remote regions (e.g. mollusks, trilobites). Such events can be attributed to global changes of

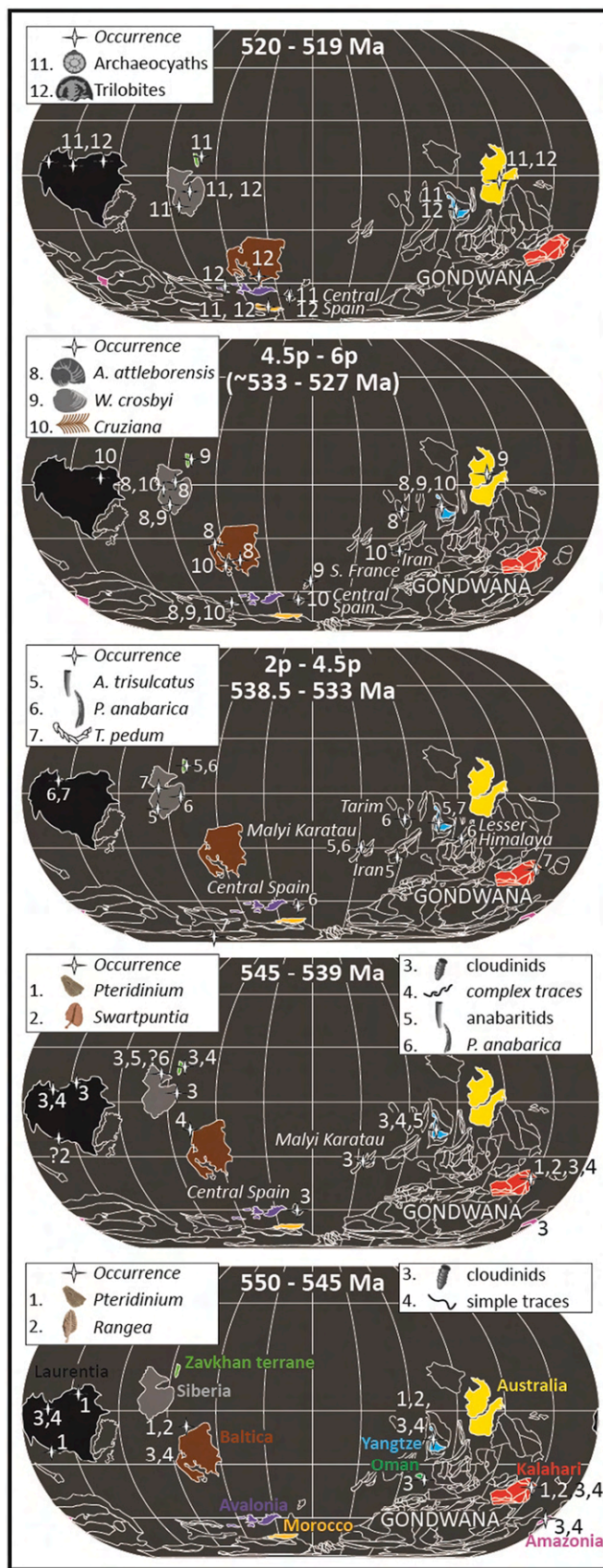


Fig. 11. Global paleobiogeography at intervals between ~ 551 and 517 Ma consistent with all age models with paleogeography after Merdith et al. (2021). Note that the positions of the Zavkhan terrane of Mongolia (bright green), Malyi Karatau of Kazakhstan, and Avalonian microcontinent in this interval remain uncertain (e.g. Landing et al., 2020). Craton coloring is consistent with stratigraphic and biostratigraphic ranges in Figs. 3-5, and 7-10. (For interpretation of the references to colour in this figure legend, the reader is referred to the web version of this article.)

environmental factors (e.g. $p\text{CO}_2$, Mg:Ca ion ratio) facilitating almost simultaneous biomineralisation of hitherto soft-bodied representatives of these groups in different basins, as noted in trilobites (Paterson et al., 2019).

We conclude that the Cambrian Explosion was in fact a protracted Ediacaran-Cambrian radiation. All models reveal widespread and correlatable late Ediacaran negative and positive $\delta^{13}\text{C}_{\text{carb}}$ excursions between ~550 Ma and the onset of the BACE. In contrast to previous studies (Amthor et al., 2003), our correlation demonstrates no significant extinction or faunal turnover coincident with the A4 anomaly, or any older negative carbon $\delta^{13}\text{C}_{\text{carb}}$ perturbation between 550 Ma and 540 Ma, but rather a series of successive, often regional, originations and minor extinctions. The canonical model (Model A) also implies that the disappearance of the Nama assemblage post-dated the BACE, whereas Model C may be compatible with a coincident disappearance of this assemblage with the BACE nadir. Regardless, the pre-BACE appearance of anabaritids and treptichnid traces in all models also argues against a global mass extinction event coincident with the BACE.

While the near synchronous global appearance of trilobites may support a calcification (biomineralisation) event in this group (Landing et al., 2020; Paterson et al., 2019), the radiation of other skeletal biota was generally highly asynchronous, with varying tempos in different basins (Figs. 8–11). This may reflect both a diversity gradient formed by clade origination in low latitudinal basins (Siberia, Mongolia, Chinese and Namibian Gondwana) and then migration to higher latitudes (e.g. Avalonia, Morocco) (Fig. 11, e.g. Jablonski et al., 2006, but see Landing et al., 2020), and also a highly heterogeneous local landscape of redox and/or nutrient regimes. The origination of many skeletal groups, including cloudinids, mollusks and trilobites, as well as the Ediacaran-Cambrian boundary itself, all seem to coincide with the succession of marked positive $\delta^{13}\text{C}_{\text{carb}}$ excursions (Figs. 9 and 10). Peak $\delta^{13}\text{C}_{\text{carb}}$ values during positive excursions during Cambrian stages 2–4 on the Siberian Platform have been proposed to record pulses of nutrients and oxygen into shallow marine seas that promoted biodiversification (He et al., 2019). By contrast, global $\delta^{13}\text{C}_{\text{carb}}$ excursions of regionally variable magnitude, from the level of the BACE to 6p, may reflect a combination of changes in glacioeustatic sea level overprinted by regional palaeomarine redox and nutrient heterogeneity. The age model framework constructed herein provides a comprehensive and editable template by which the operation of these, and other driving forces, in shaping the Ediacaran-Cambrian radiation of early animals may be explored.

Funding

FB, RW, GS, SWP, YZ and MZ acknowledge funding from the joint NERC-NSFC Biosphere Evolution Transitions and Resilience (BETR) programme (NE/P013643/1, NSFC/41661134048), MZ from the Strategic Priority Research Program (B) of the Chinese Academy of Sciences (XDB18000000, XDB 26000000), FB, SWP and GS from NERC project NE/R010129/1, and RW, SWP and FB from NERC Project NE/T008458/1. SWP acknowledges support from a Royal Society Wolfson Research Merit Award. AZ from Scientific Project 04-1-21 of the State Order of the Government of the Russian Federation to the Lomonosov Moscow State University (No. 121031600198-2). We thank C. Chilcott for technical support. We are grateful to H. Mocke and C. Hoffmann of the Geological Survey of Namibia and the Ministry of Mines and Energy, Namibia. We thank B. Romer and L. Gessert for access to Farm Swartpunt. We thank Irene Gomez Perez for enlightening discussion regarding Ara Group stratigraphy. We thank Lucas Warren and one anonymous reviewer for constructive comments and suggestions that improved the paper.

Author contributions

FB conceived the project, FB compiled all data with the help of AZ, GS, RW, CY and MZ. FB constructed the age model with insight from all

authors. FB, AC, and RW collected and analyzed Namibian samples. All authors contributed to writing the paper.

Data and materials availability

All data, including expanded geological information and full age models are available in the Supplementary Information.

Declaration of Competing Interest

The authors declare that they have no known competing financial interests or personal relationships that could have influenced the work reported in this paper.

Appendix A. Supplementary data

Supplementary data to this article can be found online at <https://doi.org/10.1016/j.earscirev.2021.103913>.

References

- Adorno, R.R., do Carmo, D.A., Germs, G., Walde, D.H.G., Denezine, M., Boggiani, P.C., Sousa e Silva, S.C., Vasconcelos, J.R., Tobias, T.C., Guimarães, E.M., Vieira, L.C., Figueiredo, M.F., Moraes, R., Caminha, S.A., Suarez, P.A.Z., Rodrigues, C.V., Caixeta, G.M., Pinho, D., Schneider, G., Muyabang, R., 2017. *Cloudina luciani* (Beurlen and Sommer, 1957), Tamengo Formation, Ediacaran, Brazil: Taxonomy, analysis of stratigraphic distribution and biostratigraphy. *Precambrian Res.* 301, 19–35.
- Ahm, A.-S.C., Bjerrum, C.J., Hoffman, P.F., Macdonald, F.A., Maloof, A.C., Rose, C.V., Strauss, J.V., Higgins, J.A., 2021. The Ca and Mg isotope record of the Cryogenian Trezona carbon isotope excursion. *Earth Planet. Sci. Lett.* 568, 117002.
- Amthor, J.E., Grotzinger, J.P., Schröder, S., Bowring, S.A., Ramezani, J., Martin, M.W., Matter, A., 2003. Extinction of *Cloudina* and *Namacalathus* at the Precambrian-Cambrian boundary in Oman. *Geology* 31, 431–434.
- An, Z., Jiang, G., Tong, J., Tian, L., Ye, Q., Song, Huyue, Song, Haijun, 2015. Stratigraphic position of the Ediacaran Miaohu biota and its constraints on the age of the upper Doushantuo $\delta^{13}\text{C}$ anomaly in the Yangtze Gorges area, South China. *Precambrian Res.* 271, 243–253. <https://doi.org/10.1016/j.precamres.2015.10.007>.
- Astakhin, V.A., Pegel, T.V., Repina, L.N., Rozanov, A.Y., Shabanov, Y.Y., Zhuravlev, A. Y., Sukhov, S.S., Sundukov, V.M., 1995. The Cambrian system of the foldbelts of Russia and Mongolia. Correlation chart and explanatory notes. *Int. Union Geol. Sci. Publ.* 32, 1–132.
- Babcock, L.E., Peng, S., Zhu, M., Xiao, S., Ahlberg, P., 2014. Proposed reassessment of the Cambrian GSSP. *J. Afr. Earth Sci.* 98, 3–10.
- Bengtson, S., Conway Morris, S., Cooper, B.J., Jell, P.A., Runnegar, B.N., 1990. Early Cambrian fossils from South Australia. *Mem. Assoc. Australas. Palaeontol.* 9, 1–364.
- Betts, M.J., Paterson, J.R., Jago, J.B., Jacquet, S.M., Skovsted, C.B., Topper, T.P., Brock, G.A., 2016. A new lower Cambrian shelly fossil biostratigraphy for South Australia. *Gondwana Res.* 36, 176–208.
- Betts, M.J., Paterson, J., Jago, J., Jacquet, S., Skovsted, C., Topper, T., Brock, G., 2017a. A new lower Cambrian shelly fossil biostratigraphy for South Australia, Reply. *Gondwana Res.* 44, 262–264.
- Betts, M.J., Paterson, J.R., Jago, J.B., Jacquet, S.M., Skovsted, C.B., Topper, T.P., Brock, G.A., 2017b. Global correlation for the early Cambrian of South Australia: Shelly fauna of the *Dailyatia odyssei* Zone. *Gondwana Res.* 46, 240–279.
- Betts, M.J., Paterson, J.R., Jacquet, S.M., Andrew, A.S., Hall, P.A., Jago, J.B., Jagodzinski, E.A., Preiss, W.V., Crowley, J.L., Brougham, T., Mathewson, C.P., Garcia-Bellido, D.C., Topper, T.P., Skovsted, C.B., Brock, G.A., 2018. Early Cambrian chronostratigraphy and geochronology of South Australia. *Earth-Sci. Rev.* 185, 498–543.
- Betts, M.J., Claybourn, T.M., Brock, G.A., Jago, J.B., Skovsted, C.B., Paterson, J.R., 2019. Shelly fossils from the lower Cambrian White Point Conglomerate, Kangaroo Island, South Australia. *Acta Palaeontol. Pol.* 64, 489–522.
- Boag, T.H., Darroch, S.A.F., Laflamme, M., 2016. Ediacaran distributions in space and time: testing assemblage concepts of earliest macroscopic body fossils. *Paleobiology* 42, 574–594.
- Bold, U., Crüger Ahm, A.S., Schrag, D.P., Higgins, J.A., Jamsran, E., Macdonald, F.A., 2020. Effect of dolomitization on isotopic records from Neoproterozoic carbonates in southwestern Mongolia. *Precambrian Res.* 350, 105902.
- Bowring, S.A., Grotzinger, J.P., Isachsen, C.E., Knoll, A.H., Pelechaty, S.M., Kolosov, P., 1993. Calibrating rates of early Cambrian evolution. *Science*. 261, 1293–1298.
- Bowring, S.A., Grotzinger, J.P., Condon, D.J., Ramezani, J., Newall, M.J., Allen, P.A., 2007. Geochronologic constraints on the chronostratigraphic framework of the Neoproterozoic Huqf Supergroup, Sultanate of Oman. *Am. J. Sci.* 307, 1097–1145.
- Brasier, M.D., Magaritz, M., Corfield, R., Luo, H., Wu, X., Ouyang, L., Jiang, Z., Hamdi, B., He, T., Fraser, A.G., 1990. The carbon- and oxygen-isotope record of the Precambrian-Cambrian boundary interval in China and Iran and their correlation. *Geol. Mag.* 127, 319–332.
- Brasier, M., Cowie, J., Taylor, M., 1994a. Decision on the Precambrian-Cambrian boundary stratotype. *Episodes* 17, 3–8.

- Brasier, M.D., Rozanov, A.Y., Zhuravlev, A.Y., Corfield, R.M., Derry, L.A., 1994b. A carbon isotope reference scale for the lower Cambrian Series in Siberia (Report of ICGP Project 303). *Geol. Mag.* 131, 767–783.
- Brasier, M.D., Shields, G., Kuleshov, V.N., Zhegallo, E.A., 1996. Integrated chemo- and biostratigraphic calibration of early animal evolution: Neoproterozoic-early Cambrian of Southwest Mongolia. *Geol. Mag.* 133, 445–485.
- Brock, G.A., Engelbreiten, M.J., Jago, J.B., Kruse, P.D., Laurie, J.R., Shergold, J.H., Shi, G.R., Sorauf, J.E., 2000. Palaeobiogeographic affinities of Australian Cambrian faunas. *Mem. Assoc. Australas. Palaeontol.* 23, 1–61.
- Bykova, N., LoDuca, S.T., Ye, Q., Marusin, V., Grazhdankin, D., Xiao, S., 2020. Seaweeds through time: Morphological and ecological analysis of Proterozoic and early Paleozoic benthic macroalgae. *Precambrian Res.* 350, 105875.
- Cai, Y., Xiao, S., Li, G., Hua, H., 2019. Diverse biomineralizing animals in the terminal Ediacaran Period herald the Cambrian explosion. *Geology* 47, 380–384. <https://doi.org/10.1130/G45949.1>.
- Chen, Z., Zhou, C., Xiao, S., Wang, W., Guan, C., Hua, H., Yuan, X., 2014. New Ediacaran fossils preserved in marine limestone and their ecological implications. *Sci. Rep.* 4, 4180.
- Chen, Z., Zhou, C., Yuan, X., Xiao, S., 2019. Death march of a segmented and trilobate bilaterian elucidates early animal evolution. *Nature* 573, 412–415. <https://doi.org/10.1038/s41586-019-1522-7>.
- Condon, D., Zhu, M., Bowring, S., Wang, W., Yang, A., Jin, Y., 2005. U-Pb ages from the neoproterozoic Doushantuo Formation, China. *Science* 308, 95–98. <https://doi.org/10.1126/science.1107765>.
- Cordie, D.R., Dornbos, S.Q., Marengo, P.J., Oji, T., Gonchigdorj, S., 2019. Depauperate skeletonized reef-dwelling fauna of the early Cambrian: insights from archaeocyathan reef ecosystems of western Mongolia. *Palaeogeogr. Palaeoclimatol. Palaeoecol.* 514, 206–221.
- Cortijo, I., Martí Mus, M., Jensen, S., Palacios, T., 2010. A new species of *Cloudina* from the terminal Ediacaran of Spain. *Precambrian Res.* 176, 1–10.
- Cui, H., Grazhdankin, D.V., Xiao, S., Peek, S., Rogov, V.I., Bykova, N.V., Sievers, N.E., Liu, X.M., Kaufman, A.J., 2016a. Redox-dependent distribution of early macroorganisms: evidence from the terminal Ediacaran Khatyspyt Formation in Arctic Siberia. *Palaeogeogr. Palaeoclimatol. Palaeoecol.* 461, 122–139. <https://doi.org/10.1016/j.palaeo.2016.08.015>.
- Cui, H., Kaufman, A.J., Xiao, S., Peek, S., Cao, H., Min, X., Cai, Y., Siegel, Z., Liu, X.M., Peng, Y., Schiffbauer, J.D., Martin, A.J., 2016b. Environmental context for the terminal Ediacaran biomineralization of animals. *Geobiology* 14, 344–363. <https://doi.org/10.1111/gbi.12178>.
- Cui, H., Xiao, S., Cai, Y., Peek, S., Plummer, R.E., Kaufman, A.J., 2019. Sedimentology and chemostratigraphy of the terminal Ediacaran Dengying formation at the Gaojiashan section, South China. *Geol. Mag.* 156, 1924–1948.
- Cui, H., Kaufman, A.J., Zou, H., Kattan, F.H., Trusler, P., Smith, J., Ivantsov, A.Y., Rich, T.H., Al Qubani, A., Yazedi, A., Lui, X.M., 2020a. Primary or secondary? A dichotomy of the strontium isotope anomalies in the Ediacaran carbonates of Saudi Arabia. *Precambrian Res.* 105720.
- Cui, H., Warren, L.V., Uhllein, G.J., Okubo, J., Liu, X.M., Plummer, R.E., Baele, J., Goderis, S., Claeys, P., Li, F., 2020b. Global or regional? Constraining the origins of the middle Bambuí carbon cycle anomaly in Brazil. *Precambrian Res.* 348, 105861.
- Daily, B., 1972. The base of the Cambrian and the first Cambrian faunas. In: Jones, J.B., McGowan, B. (Eds.), *Stratigraphic Problems of the Late Precambrian and Early Cambrian*. University of Adelaide Centre for Precambrian Research Special Paper, pp. 13–42.
- Daily, B., 1990. Cambrian stratigraphy of Yorke Peninsula. *Geol. Soc. Aust. Spec. Publ.* 16, 215–229.
- Daroch, S.A.F., Sperling, E.A., Boag, T.H., Racicot, R.A., Mason, S.J., Morgan, A.S., Tweedt, S., Myrow, P., Johnston, D.T., Erwin, D.H., Laflamme, M., 2015. Biotic replacement and mass extinction of the Ediacara biota. *Proc. R. Soc. B Biol. Sci.* 282, 20151003.
- Daroch, S.A.F., Smith, E.F., Laflamme, M., Erwin, D.H., 2018. Ediacaran extinction and Cambrian explosion. *Trends Ecol. Evol.* 33, 653–663. <https://doi.org/10.1016/j.tree.2018.06.003>.
- Daroch, S.A.F., Cribb, A.T., Buatois, L.A., Germs, G.J.B., Kenchington, C.G., Smith, E.F., Mocke, H., O'Neil, G.R., Schiffbauer, J.D., Maloney, K.M., Racicot, R.A., Turk, K.A., Gibson, B.M., Almond, J., Koester, B., Boag, T.H., Tweedt, S.M., Laflamme, M., 2021. The trace fossil record of the Nama Group, Namibia: Exploring the terminal Ediacaran roots of the Cambrian explosion. *Earth-Sci. Rev.* 212, 103435.
- Debrenne, F., Zhuravlev, A.Y., Kruse, P.D., 2015. General features of the Archaeocyatha. Systematic descriptions: Archaeocyatha. In: *Treatise on Invertebrate Paleontology, Pt. E Porifera Revised (Hypercalcified Porifera)*. Univ. Kansas Paleontol. Inst., Lawrence, KA, pp. 845–1084.
- Dilliard, K.A., Pope, M.C., Coniglio, M., Hasiotis, S.T., Lieberman, B.S., 2007. Stable isotope geochemistry of the lower Cambrian Sekwi Formation, Northwest Territories, Canada: Implications for ocean chemistry and secular curve generation. *Palaeogeogr. Palaeoclimatol. Palaeoecol.* 256, 174–194. <https://doi.org/10.1016/j.palaeo.2007.02.031>.
- Duda, J.P., Zhu, M., Reitner, J., 2016. Depositional dynamics of a bituminous carbonate facies in a tectonically induced intra-platform basin: the Shibantan Member (Dengying Formation, Ediacaran Period). *Carbonates and Evaporites* 31, 87–99. <https://doi.org/10.1007/s13146-015-0243-8>.
- Dyatlova, I.N., Sycheva, R.F., 1999. New data on lower Cambrian biostratigraphy of Eastern Sayan. *Stratigr. Geol. Korrelyatsiya* 7, 3–13.
- Gehling, J., Droser, M.L., 2013. How well do fossil assemblages of the Ediacara Biota tell time? *Geology* 41, 447–450.
- Germs, G.J.B., 1983. Implications of a sedimentary facies and depositional environmental analysis of the Nama Group in South West Africa/Namibia. *Spec. Publ. Geol. Soc. S. Afr.* 11, 89–114.
- Germs, G.J.B., Gresse, P.G., 1991. The foreland basin of the Damara and Gariep orogens in Namaqualand and southern Namibia: stratigraphic correlations and basin dynamics. *S. Afr. J. Geol.* 94 (2/3), 159–169.
- Geyman, E.C., Maloof, A.C., 2019. A diurnal carbon cycle engine explains ¹³C-enriched carbonates without increasing the global production of oxygen. *Proc. Natl. Acad. Sci. U. S. A.* 116, 24433–24439.
- Gozalo, R., Linán, E., Palacios, T., Gámez Vintaned, J.A., Mayoral, E., 2003. The Cambrian of the Iberian Peninsula: An overview. *Geol. Acta* 1, 103–112. <https://doi.org/10.1344/105.000001596>.
- Gravestock, D.I., 1984. Archaeocyatha from lower parts of the lower Cambrian carbonate sequence in South Australia. *Mem. Assoc. Australas. Palaeontol.* 2, 1–139.
- Gravestock, D.I., Alexander, E.M., Demidenco, Y.E., Esakova, N.V., Holmer, L.E., Jago, J.B., Lin, T.-R., Melnikova, L.M., Parkhaev, P.Y., Rozanov, A.Y., Ushatinskaya, G.T., Zang, W.-I., Zhegallo, E.A., Zhuravlev, A.Y., 2001. The Cambrian Biostratigraphy of the Stansbury Basin, South Australia. *Nauka, Moscow* (344p).
- Grazhdankin, D., 2004. Patterns of evolution of the Ediacaran biotas: facies versus biogeography and evolution. *Paleobiology* 30, 203–221. [https://doi.org/10.1666/0094-8373\(2004\)030<0203:podite>2.0.co;2](https://doi.org/10.1666/0094-8373(2004)030<0203:podite>2.0.co;2).
- Grazhdankin, D., 2014. Patterns of evolution of the Ediacaran soft-bodied biota. *J. Paleontol.* 88, 269–283. <https://doi.org/10.1666/13-072>.
- Gresse, P.G., Germs, G.J.B., 1993. The Nama foreland basin: sedimentation, major unconformity bounded sequences and multisided active margin advance. *Precambrian Res.* 63, 247–272. [https://doi.org/10.1016/0301-9268\(93\)90036-2](https://doi.org/10.1016/0301-9268(93)90036-2).
- Grotzinger, J.P., Bowring, S.A., Saylor, B.Z., Kaufman, A.J., 1995. Biostratigraphic and geochronological constraints on early animal evolution. *Science* 13, 229–272. <https://doi.org/10.1126/science.270.5236.598>.
- Hahn, G., Pflug, H.D., 1985. Polypentartige Organismen aus dem Jung-Präkambrium (Nama-Gruppe) von Namibia. *Geol. Palaeontol.* 19, 1–13.
- Halverson, G.P., Wade, B.P., Hurtgen, M.T., Barovich, K.M., 2010. Neoproterozoic chemostratigraphy. *Precambrian Res.* 182, 337–350. <https://doi.org/10.1016/j.precamres.2010.04.007>.
- Hay, C.C., Creveling, J.R., Hagen, C.J., Maloof, A.C., Huybers, P., 2019. A library of early Cambrian chemostratigraphic correlations from a reproducible algorithm. *Geology* 47, 457–460.
- He, T., Zhu, M., Mills, B.J.W., Wynn, P.M., Zhuravlev, A.Y., Tostevin, R., Pogge von Strandmann, P.A.E., Yang, A., Poulton, S.W., Shields, G.A., 2019. Possible links between extreme oxygen perturbations and the Cambrian radiation of animals. *Nat. Geosci.* 12, 468–474. <https://doi.org/10.1038/s41561-019-0357-z>.
- Hodgin, E.B., Nelson, L.L., Wall, C.J., Barrón-Díaz, A.J., Webb, L.C., Schmitz, M.D., Fike, D.A., Hagadorn, J.W., Smith, E.F., 2020. A link between rift-related volcanism and end-Ediacaran extinction? Integrated chemostratigraphy, biostratigraphy, and U-Pb geochronology from Sonora, Mexico. *Geology* 49, 115–119.
- Hoffman, P.F., Lamothe, K.G., 2019. Seawater-buffered diagenesis, destruction of carbon isotope excursions, and the composition of DIC in Neoproterozoic oceans. *Proc. Natl. Acad. Sci. U. S. A.* 116, 18874–18879.
- Huang, T., Chen, D., Ding, Y., Zhou, X., Zhang, G., 2020. SIMS U-Pb zircon geochronological and carbon isotope chemostratigraphic constraints on the Ediacaran-Cambrian boundary succession in the three Gorges Area, South China. *J. Earth Sci.* 31, 69–78.
- Ishikawa, T., Ueno, Y., Komiya, T., Sawaki, Y., Han, J., Shu, D., Li, Y., Maruyama, S., Yoshida, N., 2008. Carbon isotope chemostratigraphy of a Precambrian/Cambrian boundary section in the three Gorge area, South China: prominent global-scale isotope excursions just before the Cambrian explosion. *Gondwana Res.* 14, 193–208. <https://doi.org/10.1016/j.gr.2007.10.008>.
- Jablonski, D., Roy, K., Valentine, J.W., 2006. Out of the tropics: evolutionary dynamics of the latitudinal diversity gradient. *Science* 314, 102–106.
- Jago, J.B., Gehling, J.G., Betts, M.J., Brock, G.A., Dalgarno, C.R., García-Bellido, D.C., Haslett, P.G., Jacquet, S.M., Kruse, P.D., Langford, N.R., Mount, T.J., 2020. The Cambrian system in the Arrowie Basin, Flinders Ranges, South Australia. *Aust. J. Earth Sci.* 67, 923–948.
- Jensen, S., Saylor, B.Z., Gehling, J.G., Germs, G.J.B., 2000. Complex trace fossils from the terminal Proterozoic of Namibia. *Geology* 28, 143–146.
- Jiang, G., Kaufman, A.J., Christie-Blick, N., Zhang, S., Wu, H., 2007. Carbon isotope variability across the Ediacaran Yangtze platform in South China: Implications for a large surface-to-deep ocean ^δ¹³C gradient. *Earth Planet. Sci. Lett.* 261, 303–320. <https://doi.org/10.1016/j.epsl.2007.07.009>.
- Kaufman, A.J., Hayes, J.M., Knoll, A.H., Germs, G.J.B., 1991. Isotopic compositions of carbonates and organic carbon from upper Proterozoic successions in Namibia: stratigraphic variation and the effects of diagenesis and metamorphism. *Precambrian Res.* 49, 301–327. [https://doi.org/10.1016/0301-9268\(91\)90039-D](https://doi.org/10.1016/0301-9268(91)90039-D).
- Kaufman, A.J., Jacobsen, S.B., Knoll, A.H., 1993. The Vendian record of Sr and C isotopic variations in seawater: Implications for tectonics and paleoclimate. *Earth Planet. Sci. Lett.* 120, 409–430.
- Keith, M.L., Weber, J.N., 1964. Carbon and oxygen isotopic compositions of selected limestones and fossils. *Geochim. Cosmochim. Acta* 28, 1787–1816.
- Knoll, A.H., Grotzinger, J.P., Kaufman, A.J., Kolosov, P.N., 1995. Integrated approaches to terminal Proterozoic stratigraphy: An example from the Olenek Uplift, northeastern Siberia. *Precambrian Res.* 73, 251–270.
- Korobov, M.N., 1980. Lower Cambrian biostratigraphy and miomeran trilobites of Mongolia. In: Menner, V.V., Meyen, S.V. (Eds.), *Lower Cambrian and Carboniferous Biostratigraphy of Mongolia*. Sovmet. Mongol. Geol. Ekspeditsiya, Trans, 26, pp. 5–108.

- Korobov, M.N., 1989. Lower Cambrian biostratigraphy and polymeran trilobites of Mongolia. In: *Sovmest. Sov.-Mongol. Geol. Ekspeditsiya, Trans*, 48, pp. 1–204.
- Kouchinsky, A., Bengtson, S., Pavlov, V., Runnegar, B., Val'kov, A., Young, E., 2005. Pre-Tommotian age of the lower Pestrosvet Formation in the Selinde section on the Siberian platform: carbon isotopic evidence. *Geol. Mag.* 142, 319–325.
- Kouchinsky, A., Bengtson, S., Pavlov, V., Runnegar, B., Torssander, P., Young, E., Ziegler, K., 2007. Carbon isotope stratigraphy of the Precambrian-Cambrian Sukharikha River section, northwestern Siberian platform. *Geol. Mag.* 114, 1–10. <https://doi.org/10.1017/S0016756807003354>.
- Kouchinsky, A., Bengtson, S., Landing, E., Steiner, M., Vendrasco, M., Ziegler, K., 2017. Terreneuvian stratigraphy and faunas from the Anabar Uplift, Siberia. *Acta Palaeontol. Pol.* 62 <https://doi.org/10.4202/app.00289.2016>.
- Kruse, P.D., Zhuravlev, A.Y., Parkhaev, P.Y., Zhu, M., 2017. A new lower Cambrian shelly fossil biostratigraphy for South Australia. *Comment. Gondwana Res.* 44, 258–261.
- Landing, E., Kruse, P.D., 2017. Integrated stratigraphic, geochemical, and paleontological late Ediacaran to early Cambrian records from southwestern Mongolia: comment. *Geol. Soc. Am. Bull.* 129, 7–8.
- Landing, E., Schmitz, M.D., Geyer, G., Trayler, R.B., Bowring, S.A., 2020. Precise early Cambrian U-Pb zircon dates bracket the oldest trilobites and archaeocyaths in Moroccan West Gondwana. *Geol. Mag.* 158, 219–238.
- Laurie, J.R., 1986. Phosphatic fauna of the early Cambrian Todd River Dolomite, Amadeus Basin, Central Australia. *Alcheringa* 10, 431–454.
- Li, G.X., Zhao, X., Gubanov, A., Zhu, M.Y., Na, L., 2011. Early Cambrian mollusc *Watsonella crosbyi*: a potential GSSP index fossil for the base of Cambrian Stage 2. *Acta Geol. Sin.* 85, 309–319.
- Li, D., Ling, H.F., Shields-Zhou, G.A., Chen, X., Cremonese, L., Och, L., Thirlwall, M., Manning, C.J., 2013. Carbon and strontium isotope evolution of seawater across the Ediacaran-Cambrian transition: evidence from the Xiaotan section, NE Yunnan, South China. *Precambrian Res.* 225, 128–147. <https://doi.org/10.1016/j.precambres.2012.01.002>.
- Linnemann, U., Ovtcharova, M., Schaltegger, U., Gärtner, A., Hautmann, M., Geyer, G., Vickers-Rich, P., Rich, T., Plessen, B., Hofmann, M., Zieger, J., Krause, R., Kriesfeld, L., Smith, J., 2019. New high-resolution age data from the Ediacaran-Cambrian boundary indicate rapid, ecologically driven onset of the Cambrian explosion. *Terra Nova* 31, 49–58. <https://doi.org/10.1111/ter.12368>.
- Lu, M., Zhu, M., Zhang, J., Shields-Zhou, G., Li, G., Zhao, F., Zhao, X., Zhao, M., 2013. The DOUNCE event at the top of the Ediacaran Doushantuo Formation, South China: Broad stratigraphic occurrence and non-diagenetic origin. *Precambrian Res.* 225, 86–109. <https://doi.org/10.1016/j.precambres.2011.10.018>.
- Macdonald, F.A., Strauss, J.V., Sperling, E.A., Halverson, G.P., Narbonne, G.M., Johnston, D.T., Kunmann, M., Schrag, D.P., Higgins, J.A., 2013. The stratigraphic relationship between the Shuram carbon isotope excursion, the oxygenation of Neoproterozoic oceans, and the first appearance of the Ediacara biota and bilaterian trace fossils in northwestern Canada. *Chem. Geol.* 362, 250–272.
- Maloney, K.M., Boag, T.H., Faccioli, A.J., Gibson, B.M., Cribb, A., Koester, B.E., Kenchington, C.G., Racicot, R.A., Darroch, S.A.F., Laflamme, M., 2020. Palaeoenvironmental analysis of *Ermieta*-bearing Ediacaran deposits in southern Namibia. *Palaeogeogr. Palaeoclimatol. Palaeoecol.* 556, 109884.
- Malooof, A.C., Schrag, D.P., Crowley, J.L., Bowring, S.A., 2005. An expanded record of early Cambrian carbon cycling from the Anti-Atlas margin, Morocco. *Can. J. Earth Sci.* 42, 2195–2216. <https://doi.org/10.1139/e05-062>.
- Malooof, A.C., Porter, S.M., Moore, J.L., Dudás, F.O., Bowring, S.A., Higgins, J.A., Fike, D. A., Eddy, M.P., 2010. The earliest Cambrian record of animals and ocean geochemical change. *Geol. Soc. Am. Bull.* 122, 1731–1774. <https://doi.org/10.1130/B30346.1>.
- Matthews, J.J., Liu, A.G., Yang, C., McLroy, D., Levell, B., Condon, D.J., 2020. A chronostratigraphic framework for the rise of the Ediacaran microbiota: New constraints from Mistaken Point Ecological Reserve, Newfoundland. *Geol. Soc. Am. Bull.* 133, 612–624.
- Melim, L.A., Westphal, H., Swart, P.K., Eberli, G.P., Munnecke, A., 2002. Questioning carbonate diagenetic paradigms: evidence from the Neogene of the Bahamas. *Mar. Geol.* 185, 27–53.
- Merdith, A.S., Williams, S.E., Collins, A.S., Tetley, M.G., Mulder, J.A., Blades, M.L., Young, A., Armistead, S., Cannon, J., Zahirovic, S., Müller, R.D., 2021. Extending full-plate tectonic models into deep time: linking the Neoproterozoic and Phanerozoic. *Earth-Sci. Rev.* 214, 103477.
- Muscante, A.D., Bykova, N., Boag, T.H., Buatois, L.A., Mángano, M.G., Eleish, A., Prabhu, A., Pan, F., Meyer, M.B., Schiffbauer, J.D., Fox, P., Hazen, R.M., Knoll, A.H., 2019. Ediacaran biozones identified with network analysis provide evidence for pulsed extinctions of early complex life. *Nat. Commun.* 10, 1–15. <https://doi.org/10.1038/s41467-019-08837-3>.
- Narbonne, G.M., Kaufman, A.J., Knoll, A.H., 1994. Integrated chemostratigraphy and biostratigraphy of the Windermere Supergroup, northwestern Canada: Implications for Neoproterozoic correlations and the early evolution of animals. *Geol. Soc. Am. Bull.* 106, 1281–1292.
- Narbonne, G.M., Saylor, B.Z., Grotzinger, J.P., 1997. The youngest Ediacaran fossils from Southern Africa. *J. Paleontol.* 71, 953–967. <https://doi.org/10.1017/S0022336000035940>.
- Noble, S.R., Condon, D.J., Carney, J.N., Wilby, P.R., Pharaoh, T.C., Ford, T.D., 2015. U-Pb geochronology and global context of the Charnian Supergroup, UK: Constraints on the age of key Ediacaran fossil assemblages. *Geol. Soc. Am. Bull.* 127, 250–265.
- Osadchaya, D.V., Kotel'nikov, D.V., 1998. Archaeocyathids from the Atadabanian (lower Cambrian) of the Altay-Sayan Foldbelt, Russia. *Geodiversitas* 20, 5–18.
- Parkhaev, P.Y., 2019. Cambrian mollusks of Australia: Taxonomy, biostratigraphy, and Paleobiogeography. *Stratigr. Geol. Correl.* 27, 181–206.
- Parkhaev, P.Y., Karlova, G.A., 2011. Taxonomic revision and evolution of Cambrian molluscs of the genus *Aldanella* Vostokova, 1962 (Gastropoda: Archaeobranchia). *Paleontol. J.* 45, 1145–1205.
- Parry, L.A., Boggiani, P.C., Condon, D.J., Garwood, R.J., de Leme, J.M., McLroy, D., Brasier, M.D., Trindade, R., Capanha, G.A.C., Pacheco, M.L.A.F., Diniz, C.Q.C., Liu, A., 2017. Ichnological evidence for meiofaunal bilaterians from the terminal Ediacaran and earliest Cambrian of Brazil. *Nat. Ecol. Evol.* 1, 1455–1464.
- Paterson, J.R., Edgecombe, G.D., Lee, M.S., 2019. Trilobite evolutionary rates constrain the duration of the Cambrian explosion. *Proc. Natl. Acad. Sci. U. S. A.* 116, 4394–4399.
- Pelechaty, S.M., 1998. Integrated chronostratigraphy of the Vendian System of Siberia: implications for a global stratigraphy. *Geol. Soc. Lond.* 155, 957–973.
- Pelechaty, S.M., Grotzinger, J.P., Kashirtsev, V.A., Zhernovskiy, V.P., 1996a. Chemostratigraphic and sequence stratigraphic constraints on Vendian-Cambrian basin dynamics, Northeast Siberian Craton. *J. Geol.* 104, 543–563.
- Pelechaty, S.M., Kaufman, A.J., Grotzinger, J.P., 1996b. Evaluation of $\delta^{13}\text{C}$ chemostratigraphy for intrabasinal correlation: Vendian strata of Northeast Siberia. *Bull. Geol. Soc. Am.* 108, 992–1003. [https://doi.org/10.1130/0016-7606\(1996\)108<0992:E0CCCF>2.3.CO;2](https://doi.org/10.1130/0016-7606(1996)108<0992:E0CCCF>2.3.CO;2).
- Pickford, M.H.L., 1995. Review of the Riphean, Vendian and early Cambrian palaeontology of the Otavi and Nama groups, Namibia. *Commun. Geol. Surv. Namibia* 10, 57–81.
- Porter, S.M., 2007. Seawater chemistry and early carbonate biomineralization. *Science* 316, 1302.
- Prave, A.R., Kirsimäe, K., Lepland, A., Fallick, A.E., Kreitsmann, T., Deines, Y.E., Romashkin, A.E., Rychanchik, D.V., Medvedev, P.V., Moussavou, M., Bakakas, K., 2021. The grandest of them all: the Lomagundi-Jatuli Event and Earth's oxygenation. *J. Geol. Soc. Lond.* 179 (1), jgs2021-036. <https://doi.org/10.1144/jgs2021-036>.
- Rogov, V.I., Karlova, G.A., Marusin, V.V., Kochnev, B.B., Nagovitsin, K.E., Grazhdankin, D.V., 2015. Duration of the first biozone in the Siberian hypostrototype of the Vendian. *Russ. Geol. Geophys.* 56, 573–583.
- Rooney, A.D., Cantine, M.D., Bergmann, K.D., Gómez-Pérez, I., Al Baloushi, B., Boag, T. H., Busch, J.F., Sperling, E.A., Strauss, J.V., 2020. Calibrating the coevolution of Ediacaran life and environment. *Proc. Natl. Acad. Sci. U. S. A.* 117, 16824–16830.
- Saylor, B.Z., 2003. Sequence stratigraphy and carbonate-siliciclastic mixing in a terminal Proterozoic foreland basin, Urusis Formation, Nama Group, Namibia. *J. Sediment. Res.* 73, 264–279. <https://doi.org/10.1306/082602730264>.
- Saylor, Beverly Z., Grotzinger, J.P., 1996. Reconstruction of important Proterozoic-Cambrian boundary exposures through the recognition of thrust deformation in the Nama Group of southern Namibia. *Commun. Geol. Surv. Namibia* 11, 1–12.
- Saylor, B.Z., Grotzinger, J.P., Germs, G.J.B., 1995. Sequence stratigraphy and sedimentology of the Neoproterozoic Kuibis and Schwartrand Subgroups (Nama Group), southwestern Namibia. *Precambrian Res.* 73, 153–171. [https://doi.org/10.1016/0301-9268\(94\)00076-4](https://doi.org/10.1016/0301-9268(94)00076-4).
- Saylor, B.Z., Kaufman, A.J., Grotzinger, J.P., Urban, F., 1998. A composite reference section for terminal Proterozoic strata of southern Namibia. *J. Sediment. Res.* 68, 1223–1235. <https://doi.org/10.2110/jsr.68.1223>.
- Schmitz, M.D., 2012. Radiogenic isotope geochronology. In: Gradstein, F.M., Ogg, J.G., Schmitz, M.D., Ogg, G.M. (Eds.), *The Geological Time Scale 2012*. Elsevier, pp. 115–126.
- Smith, O., 1998. Terminal Proterozoic Carbonate Platform Development: Stratigraphy and Sedimentology of the Kuibis Subgroup (ca. 550–548 Ma). Massachusetts Institute of Technology, Northern Nama Basin, Namibia.
- Smith, E.F., Macdonald, F.A., Petach, T.A., Bold, U., Schrag, D.P., 2015. Integrated stratigraphic, geochemical, and paleontological late Ediacaran to early Cambrian records from southwestern Mongolia. *Geol. Soc. Am. Bull.* 128, 442–468. <https://doi.org/10.1130/B31248.1>.
- Smith, E.F., Nelson, L.L., Strange, M.A., Eyster, A.E., Rowland, S.M., Schrag, D.P., Macdonald, F.A., 2016. The end of the Ediacaran: two new exceptionally preserved body fossil assemblages from Mount Dunfee, Nevada, USA. *Geology* 44, 911–914. <https://doi.org/10.1130/G38157.1>.
- Steiner, M., Yang, B., Hohl, S., Zhang, L., Chang, S., 2020. Cambrian small skeletal fossil and carbon isotope records of the southern Huangling Anticline, Hubei (China) and implications for chemostratigraphy of the Yangtze Platform. *Palaeogeogr. Palaeoclimatol. Palaeoecol.* 554, 109817.
- Tahata, M., Ueno, Y., Ishikawa, T., Sawaki, Y., Murakami, K., Han, J., Shu, D., Li, Y., Guo, J., Yoshida, N., Komiya, T., 2013. Carbon and oxygen isotope chemostratigraphies of the Yangtze platform, South China: Decoding temperature and environmental changes through the Ediacaran. *Gondwana Res.* 23, 333–353. <https://doi.org/10.1016/j.gr.2012.04.005>.
- Uhlein, G.J., Uhlein, A., Pereira, E., Caxito, F.A., Okubo, J., Warren, L.V., Sial, A.N., 2019. Ediacaran paleoenvironmental changes recorded in the mixed carbonate-siliciclastic Bambuí Basin, Brazil. *Palaeogeogr. Palaeoclimatol. Palaeoecol.* 517, 39–51.
- Veizer, J., Hoefs, J., 1976. The nature of $^{18}\text{O}/^{16}\text{O}$ and $^{13}\text{C}/^{12}\text{C}$ secular trends in sedimentary carbonate rocks. *Geochim. Cosmochim. Acta* 40, 1387–1395.
- Veizer, J., Holser, W.T., Wilgus, C.K., 1980. Correlation of $^{13}\text{C}/^{12}\text{C}$ and $^{34}\text{S}/^{32}\text{S}$ secular variations. *Geochim. Cosmochim. Acta* 44, 579–587.
- Vernhet, E., 2007. Paleobathymetric influence on the development of the late Ediacaran Yangtze platform (Hubei, Hunan, and Guizhou provinces, China). *Sediment. Geol.* 197, 29–46.
- Vishnevskaya, I.A., Kochnev, B.B., Letnikova, E.F., Kiseleva, V.Y., Pisareva, N.I., 2013. Sr isotope signatures in the Vendian Khorbusunoka Group of the Olenek Uplift (northeastern Siberian Platform). *Dokl. Earth Sci.* 449, 298–302.

- Vishnevskaya, I.A., Letnikova, E.F., Vetrova, N.I., Kochnev, B.B., Dil, S.I., 2017. Chemostratigraphy and detrital zircon geochronology of the Neoproterozoic Khorbusuonka Group, Olenek Uplift, Northeastern Siberian platform. *Gondwana Res.* 51, 255–271.
- Wang, W., Zhou, C., Guan, C., Yuan, X., Chen, Z., Wan, B., 2014. An integrated carbon, oxygen, and strontium isotopic studies of the Lantian Formation in South China with implications for the Shuram anomaly. *Chem. Geol.* 373, 10–26. <https://doi.org/10.1016/j.chemgeo.2014.02.023>.
- Wang, W., Guan, C., Zhou, C., Peng, Y., Pratt, L.M., Chen, X., Chen, L., Chen, Z., Yuan, X., Xiao, S., 2017. Integrated carbon, sulfur, and nitrogen isotope chemostratigraphy of the Ediacaran Lantian Formation in South China: Spatial gradient, ocean redox oscillation, and fossil distribution. *Geobiology* 15, 552–571. <https://doi.org/10.1111/gbi.12226>.
- Warren, L.V., Fairchild, T.R., Gaucher, C., Boggiani, P.C., Poiré, D.G., Anelli, L.E., Inchausti, J.C.G., 2011. *Corumbella* and in situ *Cloudina* in association with thrombolites in the Ediacaran Itapucumi Group, Paraguay. *Terra Nova* 23, 382–389. <https://doi.org/10.1111/j.1365-3121.2011.01023.x>.
- Warren, L.V., Buatois, L., Mangano, M.G., Simões, M.G., Santos, M.G.M., Poiré, D., Riccomini, C., Assine, M.L., 2020. Microbially induced pseudotraces from a Pantanal soda lake, Brazil: Alternative interpretations for Ediacaran simple trails and their limits. *Geology* 48, G472341.
- Wood, R.A., Poulton, S.W., Prave, A.R., Hoffmann, K.-H., Clarkson, M.O., Guilbaud, R., Lyne, J.W., Tostevin, R., Bowyer, F., Penny, A.M., Curtis, A., Kasemann, S.A., 2015. Dynamic redox conditions control late Ediacaran metazoan ecosystems in the Nama Group, Namibia. *Precambrian Res.* 261, 252–271. <https://doi.org/10.1016/j.precamres.2015.02.004>.
- Wood, R.A., Liu, A.G., Bowyer, F.T., Wilby, P.R., Dunn, F.S., Kenchington, C.G., Hoyal Cuthill, J.F., Mitchell, E.G., Penny, A.M., 2019. Integrated records of environmental change and evolution challenge the Cambrian Explosion. *Nat. Ecol. Evol.* 3, 528–538.
- Xiao, S.H., Narbonne, G.M., 2020. The Ediacaran period. In: Gradstein, F.M., Ogg, J.G., Schmitz, M.D., Ogg, G.M. (Eds.), *Geological Time Scale 2020*. Elsevier B.V, pp. 521–561.
- Xiao, S., Chen, Z., Pang, K., Zhou, C., Yuan, X., 2020. The Shibantan Lagerstätte: insights into the Proterozoic-Phanerozoic transition. *J. Geol. Soc. Lond.* 178.
- Yang, A., Zhu, M., Zhuravlev, A.Y., Yuan, K., Zhang, J., Chen, Y., 2016a. Archaeocyathan zonation of the Yangtze Platform: implications for regional and global correlation of lower Cambrian stages. *Geol. Mag.* 153, 388–409.
- Yang, B., Steiner, M., Zhu, M., Li, G., Liu, J., Liu, P., 2016b. Transitional Ediacaran–Cambrian small skeletal fossil assemblages from South China and Kazakhstan: Implications for chronostratigraphy and metazoan evolution. *Precambrian Res.* 285, 202–215.
- Yang, C., Rooney, A.D., Condon, D.J., Li, X.-H., Grazhdankin, D.V., Bowyer, F.T., Hu, C., Macdonald, F., Zhu, M., 2021. The tempo of Ediacaran evolution. *Sci. Adv.* 7 (45), eabi9643.
- Zhou, C., Xiao, S., Wang, W., Guan, C., Ouyang, Q., Chen, Z., 2017. The stratigraphic complexity of the middle Ediacaran carbon isotopic record in the Yangtze Gorges area, South China, and its implications for the age and chemostratigraphic significance of the Shuram excursion. *Precambrian Res.* 288, 23–38. <https://doi.org/10.1016/j.precamres.2016.11.007>.
- Zhu, M., Zhang, J., Yang, A., 2007. Integrated Ediacaran (Sinian) chronostratigraphy of South China. *Palaeogeogr. Palaeoclimatol. Palaeoecol.* 254, 7–61. <https://doi.org/10.1016/j.palaeo.2007.03.025>.
- Zhu, M., Lu, M., Zhang, J., Zhao, F., Li, G., Aihua, Y., Zhao, X., Zhao, M., 2013. Carbon isotope chemostratigraphy and sedimentary facies evolution of the Ediacaran Doushantuo Formation in western Hubei, South China. *Precambrian Res.* 225, 7–28. <https://doi.org/10.1016/j.precamres.2011.07.019>.
- Zhu, M., Zhuravlev, A.Y., Wood, R.A., Zhao, F., Sukhov, S.S., 2017. A deep root for the Cambrian explosion: Implications of new bio- and chemostratigraphy from the Siberian Platform. *Geology* 45, 459–462.
- Zhuravlev, A.Y., 1998. Early Cambrian archaeocyathan assemblages of Mongolia. *Lund Publ. Geol.* 142, 24–25.
- Zhuravlev, A.Y., Gravestock, D.I., 1994. Archaeocyaths from Yorke Peninsula, South Australia and archaeocyathan early Cambrian zonation. *Alcheringa* 18, 1–54.
- Zhuravlev, A.Y., Naimark, E.B., 2005. Alpha, beta, or gamma: Numerical view on the early Cambrian world. *Palaeogeogr. Palaeoclimatol. Palaeoecol.* 220, 207–225.
- Zhuravleva, I.T., Konyaeva, I.A., Osadchaya, D.V., Boyarinov, A.S., 1997. Biostratigraphy of the Kiya River section. Early Cambrian archaeocyaths and spicular sponges from the Kiya River section (Kuznetsk Alatau). *Ann. Paleontol.* 83, 115–200.